

Raman spectroscopic investigation of two grains from comet 81P/Wild 2: Information that can be obtained beyond the presence of sp²-bonded carbon

Brigitte WOPENKA

Department of Earth and Planetary Sciences and McDonnell Center for the Space Sciences, Washington University,
St. Louis, Missouri 63130–4899, USA
E-mail: bwopenka@levee.wustl.edu

(Received 15 July 2011; revision accepted 10 November 2011)

Abstract—Raman analyses were performed of individual micrometer-sized fragments of material returned to Earth by the NASA Stardust mission to comet 81P/Wild 2. The studied fragments originated from grains (C2054,0,35,91,0 and C2092,6,80,51,0) of two different penetration tracks that occurred in two different silica aerogel collector cells. All fragments of both particles have Raman spectra characteristic of amorphous sp²-bonded carbon that are in general agreement with the results published in previous Stardust particle studies. The present study, however, does not focus on the discussion of specific details of the D and G band parameters, but rather reports on additional information that can be obtained from returned Stardust samples via Raman spectroscopy. Most notably, the Raman spectra show that all analyzed fragments of the particles were contaminated with the capture medium (i.e., aerogel). The silica aerogel is laced with organic aliphatic and aromatic hydrocarbon impurities that resulted in strong bands in the ~ 2900 Δcm⁻¹ spectral range (C-H stretching modes). Aerogel bands are also found in the 1000–1600 Δcm⁻¹ spectral range, where they overlap with the bands of the amorphous sp²-bonded carbon. The peaks associated with the aerogel contamination differ between the two grains that originated from two different aerogel cells. In addition to the bands due to aerogel contamination and the always present sp²-bonded carbon bands, fragments of particle C2092,6,80,51,0 also show Raman peaks for pyrrhotite and Fa₃₀ Fo₇₀ olivine. Complete (up to 4000 Δcm⁻¹) raw and baseline-corrected Raman spectra of the Stardust particles are shown and discussed in detail.

INTRODUCTION

The comet sample return mission to comet 81P/Wild 2 (i.e., the NASA Stardust mission) was launched by NASA in 1999. The mission collected ejected comet dust during its encounter with comet 81P/Wild 2 when it flew past the comet at 1.86 AU from the Sun with a relative encounter speed of 6.1 km s⁻¹. This flyby and dust collection occurred in 2004 when the spacecraft was 390 million km away from Earth. The comet dust particles were captured (i.e., collected by impact) in ultralow density (0.01–0.05 g cm⁻³) amorphous SiO₂-based (i.e., silica) aerogel cells that were mounted on a modular grid-like collector tray (Brownlee et al. 2003, 2006).

Each aerogel cell was 40 × 20 mm in size and 30 mm deep, and there were a total of 132 individual rectangular

aerogel cells on the collector tray (Tsou et al. 2004). This collection method (i.e., capture in aerogel cells, which consist of 99.9 vol% air and 0.1 vol% SiO₂) was chosen to minimize particle heating that could potentially occur during the hypervelocity impact of the dust at 6.1 km s⁻¹ (Tsou 1995). The sample trays with the aerogel collectors (which have experienced 7 yr of vacuum in space) were successfully returned to Earth in January 2006 and since then have been guarded, documented, and studied by the staff of the curatorial facility at the NASA Johnson Space Center (JSC). At JSC, the exposed surfaces of the cells were analyzed for impacts, and thousands of particles < 100 μm in size were photographically documented. Selected impacts (tracks) were subjected to “microsurgery” in order to make cometary material available for distribution to scientists for analysis. This was done

according to a protocol that was essentially a “hierarchy of dissection”: tracks were dissected from cells, grains were dissected from tracks, and slices and fragments were dissected from grains and nanogram-sized samples were embedded and mounted in preparation for analyses by many different analytical techniques (Zolensky et al. 2008).

The path or cavity left in the aerogel by the impacting particle is called impact track and can range from tens of micrometers to millimeters in size. The penetration tracks can have various forms, which were studied and documented in detail over the last several years (e.g., Hörz et al. 2006). Most of the penetration tracks are bulb-shaped at first (i.e., close to the entrance location into the aerogel) and then peter out into tails of various lengths. Most of the tracks contain particle fragments along their bulb-shaped walls, and such fragments coming from two different bulb-shaped penetration holes were studied in the present work.

Previous Raman spectroscopic studies of Stardust particles reported on the presence and interpretation of the two broad bands that are caused by amorphous sp^2 -bonded carbon (typically referred to as D and G bands). So far the D and G bands were detected in the spectra of all Raman-analyzed Stardust particles (except the ones reported in Bridges et al. 2010), and they are also present in the spectra of the present study. Most Raman studies on Stardust grains focus on the quantitative interpretation of the sp^2 -bonded carbon spectra, which is based on peak deconvolutions of the carbon D and G bands (e.g., Sandford et al. 2006; Muñoz-Caro et al. 2008; Rotundi et al. 2008). While this quantitative Raman peak analysis is of interest and relevant to the understanding of the nature of organics in comets as well as in interplanetary dust particles (IDPs) (e.g., Quirico et al. 2005; Muñoz-Caro et al. 2006; Busemann et al. 2009; Brunetto et al. 2011) and meteorites (e.g., Bonal et al. 2006; Busemann et al. 2007), it is not the focus of the present study. Rather, the purpose of the present study is to discuss what information Raman spectroscopy can provide about 81P/Wild 2 Stardust particles that goes beyond the previously well-documented fact that the particles contain amorphous sp^2 -bonded carbonaceous material. Another purpose of this article is to publish the actual Raman spectra of Stardust particles (rather than only peak deconvolution results of the D and G bands) in the complete spectral range from 100 to 4000 cm^{-1} . This not only allowed for the identification of minerals and the detection of contamination due to aerogel (see below), but such detailed spectra also might be of interest to scientists who have used (or will use) complementary analytical techniques to study returned Stardust particles.

EXPERIMENTAL PROCEDURES

Samples Received from NASA

Particle extraction from the returned Stardust collection trays was performed by the NASA curatorial staff. Individual Stardust tracks were isolated as so-called “keystones” from their aerogel cells (Westphal et al. 2004). After photodocumentation and optical examination, large individual grains were isolated and extracted from the capture tracks by NASA. Gold mounts had been prepared and provided by Washington University and sent to NASA’s curatorial staff. Two grains were selected from tracks in two different cells and extracted from their keystones. The grains were each put in one of the $10 \times 10 \text{ mm}$ squares of two different flat Au mounts and photodocumented. The particles were then pressed into the gold mount in order to provide a good heat sink when the sample is being irradiated by the laser during Raman analysis. After being pressed into the Au mount, the samples were photographed again.

While the topography of the sample surface is not important for traditional Raman microprobe analysis (i.e., flattening of the sample is generally not necessary), the pressing of the sample on the Au mount has the advantage that a good thermal contact is made between sample and substrate. In addition, Au is an ideal sample mounting material, because it has no Raman spectrum on its own. The technique of particle flattening (i.e., the pressing) was previously used as sample preparation for Raman analysis of IDPs (Wopenka 1988), and is described in detail in Zolensky et al. (2008).

Grain #91 comes from track #35 in aerogel cell #C2054 (Fig. 1a). Before the grain was pressed into the Au mount it had a size of $\sim 10 \times 7 \text{ }\mu\text{m}$, and after pressing it spread out over an area of $\sim 20 \times \sim 10 \text{ }\mu\text{m}$, and split into several larger fragments (see Fig. 2). Individual spots of $\sim 1 \text{ }\mu\text{m}$ diameter were selected for Raman analysis (see Fig. 3). Grain #51 comes from track #80 in aerogel cell #C2092 (Fig. 1b). Before the grain was pressed into the Au mount it was already spread out into many different small fragments that were embedded in aerogel (see Fig. 2 bottom “before pressing”). After the sample was pressed into the Au substrate, the particle fragments spread out even more over an area of $\sim 100 \times 100 \text{ }\mu\text{m}$ (see Fig. 2 bottom “after pressing”), and Raman analysis could be performed in individual micrometer-sized areas of the particle.

Raman Microprobe Spectroscopy

Traditional Raman spectra (as opposed to Raman maps or Raman images) were obtained in the complete

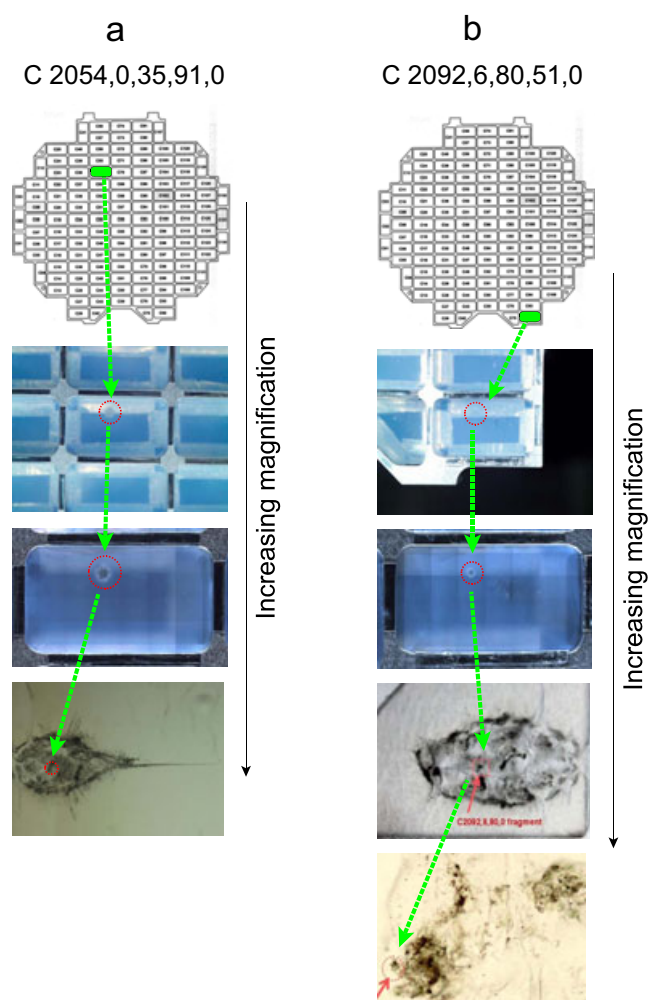


Fig. 1. Capture locations of Stardust grains analyzed in this study. Top row: Sketch of cometary collector tray C2 showing the layout of the 132 aerogel cells and the capture locations of cells C2054 and C2092. Other rows: Optical micrographs showing zoom-ins into the aerogel cells and details of the tracks. Individual photos are from the NASA Curator Website http://curator.jsc.nasa.gov/stardust/sample_catalog/. a) Grain C2054,0,35,91,0. Track #35 is a type B track and exhibits the typical lateral spreading of the cometary material in the aerogel after its entry. Subsequent vaporization of the material produced the characteristic bulb (Burchell et al. 2008; Trigo-Rodríguez et al. 2008; Zolensky et al. 2008). The location of grain #91 that was isolated and mounted for subsequent Raman analysis is within the red circle in the bottom micrograph (see details in Fig. 2). b) Grain C2092,6,80,51,0. Track #80, which is a borderline type B/C track (Trigo-Rodríguez et al. 2008), also exhibits the typical lateral spreading of the cometary material in the aerogel after its entry. The bottom micrograph shows a detailed view of track #80 and the capture location of grain #51 (within the red circle) that was isolated and mounted for subsequent Raman analysis (see details in Fig. 2).

relative wavenumber range from 100 to $4000 \Delta\text{cm}^{-1}$ from optically preselected, photodocumented micrometer-sized spots of the samples. Those Raman measurements

were performed with the HoloLab 5000 Raman Microscope from Kaiser Optical Systems, Inc., which is an integrated, fiber-optically coupled confocal microscope–spectrometer–detector system. This instrument has no moving parts and is based on an axial spectrometer with holographic gratings that allows for very good photon efficiency and wavelength accuracy. Raman peak positions can be measured with $\pm 0.5 \text{ cm}^{-1}$ accuracy. Raman excitation light of 532 nm ($18,976 \text{ cm}^{-1}$) from a frequency-doubled Nd-YAG laser is delivered via an $8 \mu\text{m}$ single-mode optical fiber that is coupled into a Leica research-grade DML microscope (Leitz, Wetzlar, Germany).

This confocal microscope is equipped with both transmission and reflection optics and is integrated with a Kaiser Holographic FC probe head and a digital video assembly. The sample can be viewed in reflected or transmitted light, and individual micrometer-sized areas can be selected (and photodocumented) for Raman analysis. In the case of this study, the individual samples could be viewed only in reflected light, because they were mounted on a gold substrate. A $80\times$ ULWD objective (Olympus, Japan) with numerical aperture of 0.75 and a working distance of 8 mm was used for focusing the light onto the sample, which resulted in a laser spot size (and thus a spatial resolution) of $\sim 1 \mu\text{m}$. The laser power at the surface of the sample can be adjusted between 0.1 and 10 mW, and was $< 0.5 \text{ mW}$ for the analysis of the samples in this study. However, because the laser is focused through the microscope objective to $\sim 1 \mu\text{m}$ diameter, the resultant power density (and thus the heat created) can still be substantial, and the degree of heating will depend on the thermal conductivity of the sample and its mounting medium. Thus, it helps to press the samples in a material that has good thermal conductivity and can provide a good heat sink, such as gold. When this is done and low laser powers are used, the technique is typically nondestructive to the sample, which means that the samples usually will be available for other analytical techniques after Raman analysis. However, some very heat-sensitive samples (such as biological samples, some organics, and some forms of amorphous sp^2 -bonded carbon materials) can be destroyed, even with reduced laser power and ideal sample preparation. Thus, there is never a 100% guarantee that a heat-sensitive sample will survive the Raman analysis. Especially for heat-sensitive samples it is therefore important to photographically document the samples before and after Raman analysis to ensure that no damage has occurred to the sample during the Raman analysis.

The backscattered light (including the Raman scattered light) is collected through the same $80\times$ objective that is used to focus the exciting laser beam,

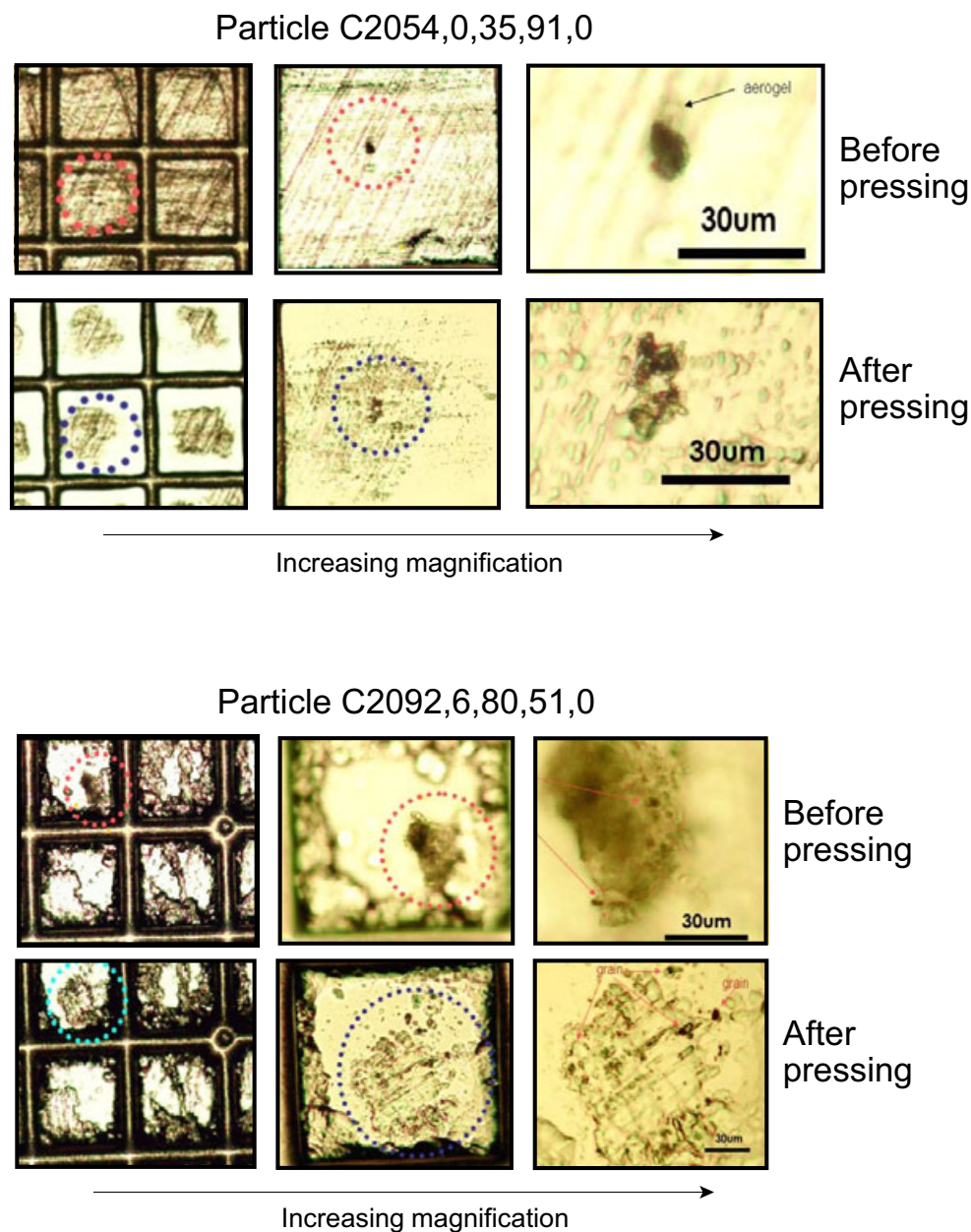


Fig. 2. Optical microscope images of Stardust particles C2054,0,35,91,0 and C2092,6,80,51,0 mounted on Au substrate in preparation for Raman analysis. The grains were removed by the NASA curatorial staff from their tracks and pressed in Au mounts that were provided by Washington University. The exact locations and appearances of the particles were photodocumented before and after pressing them into the Au mounts. Individual photos documenting the sample preparation procedures were obtained and provided by the NASA curatorial staff.

focused onto the core of a 100 μm multimode optical collection fiber, and guided into the spectrometer that is configured with a Holoplex transmission grating (HPG-532). The beam passes through a holographic element of the $f/1.8$ holographic imaging spectrograph and splits into two parts that are then imaged onto a thermoelectrically cooled CCD array detector (Andor Technology) with 2048 channels. The spectrometer geometry

is such that the upper portion of the pixels images 100–2500 Δcm^{-1} , whereas the lower portion of the pixels images 2200–4400 Δcm^{-1} . Thus, although the spectral resolution is $\sim 2.5 \text{ cm}^{-1}$ (i.e., our resolution is $\sim 1 \text{ cm}^{-1} \text{ pixel}^{-1}$), the whole spectral range of interest in Raman spectroscopy from 100 to 4200 Δcm^{-1} (corresponding to 534–685 nm with 532 nm excitation) can be detected simultaneously.

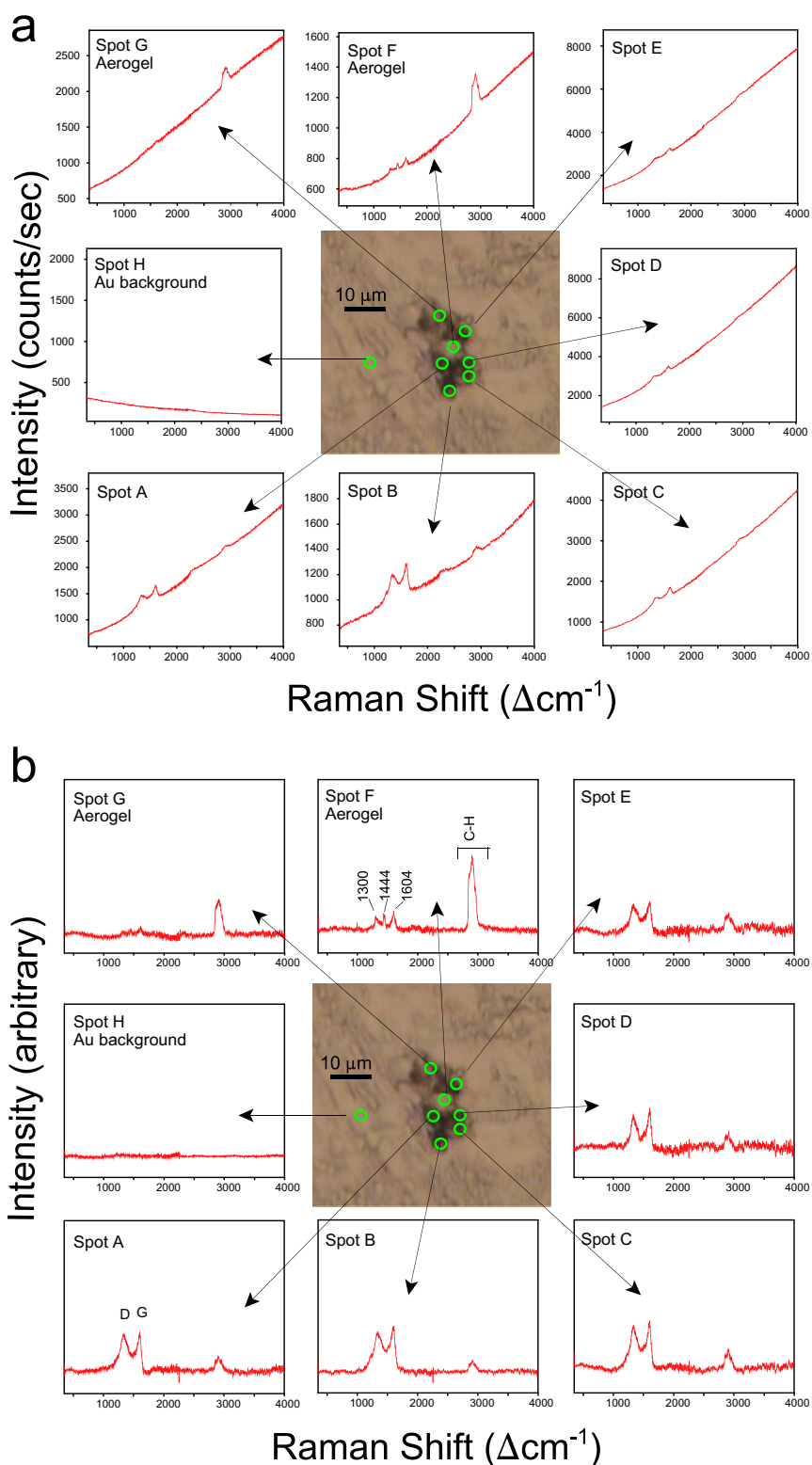


Fig. 3. Full Raman spectra ($350\text{--}4000\ \Delta\text{cm}^{-1}$) of seven different selected micrometer-sized spots of Stardust particle C2054,0,35,91,0 pressed into gold. The spectrum of the mounting medium (spot H) is also shown. The particle is seen in the Raman microprobe as a rotated (by 180°) mirror image compared to the way it is shown in Fig. 2. a) Raw Raman spectra without any background correction or any other spectral manipulation. The raw spectra are dominated by fluorescence. b) Baseline-corrected spectra. The Raman spectral details only become obvious after baseline correction.

Spectral acquisition time was 64×4 s per spectrum. Each optically selected micrometer-sized spot was analyzed three to five times (after defocusing and refocusing on the area of interest) to confirm that the spectra were representative of a given individual spot (which they usually were). Data acquisition, intensity and wavelength calibration, cosmic ray filtering, as well as data manipulation (such as baseline correction and peak deconvolution) were all controlled by the GRAMS32™ V. 4.0 data collection software by Galactic.

Representative spectra of individual spots in the two Stardust particles analyzed are shown below. The spectra are plotted either as raw spectra or as baseline-corrected spectra. Raw spectra have true count rates on the y -axis labels of the figures, and thus not only give information about the Raman bands but also about the laser-induced fluorescence of the sample. The latter is manifested in high background count rates that typically increase with increasing relative wavenumber, which makes it difficult (and sometimes even impossible) to see the superimposed Raman bands. However, the background (whether steep or subtle) that is underlying the Raman signals can be corrected with an operator-controlled manual multipoint (as needed, up to 10 points) linear baseline correction algorithm over the entire acquired spectral range, which makes it easier to both see and identify the Raman peaks and compare spectra from different spots and/or different samples. As both the raw spectra as well as the baseline-corrected spectra can contain important analytical information, examples of both types of spectra are shown for the Stardust particles analyzed in this study. Each spot was analyzed three to five times to confirm that the obtained spectra are representative of individual spots (which they were). The state of the Stardust samples post-Raman analysis seems to be unchanged compared with their pre-Raman analysis state, i.e., no damage occurred to the samples during Raman analysis. At least, there was no damage that could have been visually recognized via optical microscopy.

RESULTS

Stardust Sample C2054,0,35,91,0

After being pressed into Au, the grain split into fragments and spread out over an area of $\sim 20 \times \sim 10$ μm . A total of 10 different micrometer-sized spots in different areas of the particle were analyzed. Figure 3a shows the Raman spectra of seven representative analyzed spots (spots A–G) as well as the spectrum of the Au mounting medium (spot H). Those raw spectra show actual count rates on the y -axes, i.e., the kind of spectra that are acquired/obtained before any follow-up spectral manipulations or baseline corrections is performed.

Spots A–E were dark areas (i.e., fragments of the actual particle), whereas spots F and G were areas that appeared colorless in reflected light. No Raman peaks and no fluorescence were observed for the Au substrate away from the sample (spot H), which means that the strong fluorescence (which is observed in all other spectra of this particle) is associated with the particle and/or the aerogel of cell C2054, which sticks to the sample.

Spots A–E all show the characteristic Raman spectrum of amorphous sp^2 -bonded carbon, i.e., the very wide bands centered at ~ 1350 and ~ 1600 Δcm^{-1} . These two bands have traditionally been called D band (for disorder), and G band (for graphite), because they also occur (but with substantially narrower peaks!) in graphitic (i.e., crystalline) sp^2 -bonded materials. Because those Raman bands are superimposed on steep fluorescence backgrounds, the raw spectra of different spots (Fig. 3a) can look quite different. The background count rates can be quite variable, as seen on the different numbers on the y -axis labels of the spectra. The higher the fluorescence background, the more difficult it is to see the superimposed Raman bands in the raw spectra. It is not known why different micrometer-sized spots of the opaque particle have such different backgrounds (i.e., photo-induced fluorescence), but repeated analyses of the same spots (after moving the sample away from the laser beam and back again and refocusing the laser beam on the spot) yield the same results. Spots F and G show very different kinds of spectra (i.e., they do not show the bands related to the sp^2 -bonded carbon, which is obvious even in the raw spectra), and are most likely representative of the aerogel that sticks to the particle. The spectra of spots F and G have also very strong fluorescence, so that the cause for the fluorescence must be associated with the aerogel (and maybe, in addition, with the particle). Most notably, however, the spectra of spots F and G have very prominent peaks in the C-H stretching region at ~ 2900 Δcm^{-1} , in addition to several weaker peaks in the 1300–1600 Δcm^{-1} region.

Because of differences in the background count rate, the broad bands caused by the sp^2 -bonded carbon can look quite different in the raw spectra (e.g., compare spectra of spots B and D in Fig. 3a). Spectra in the low wavenumber region for all spots that show D and G bands are compared in Figs. 4a and 4b. The fact that the Raman spectra from spots A through E are indeed identical (or at least very similar) becomes much more obvious once a baseline suppression is applied to correct for the fluorescence background (Figs. 3b and 4c). Those baseline-corrected Raman spectra plotted with arbitrary intensities are clearly showing the following: (1) no peaks are detected in the Au mount spectrum (spot H), (2) the dark-colored (i.e., black) areas (spots A–E) all show the

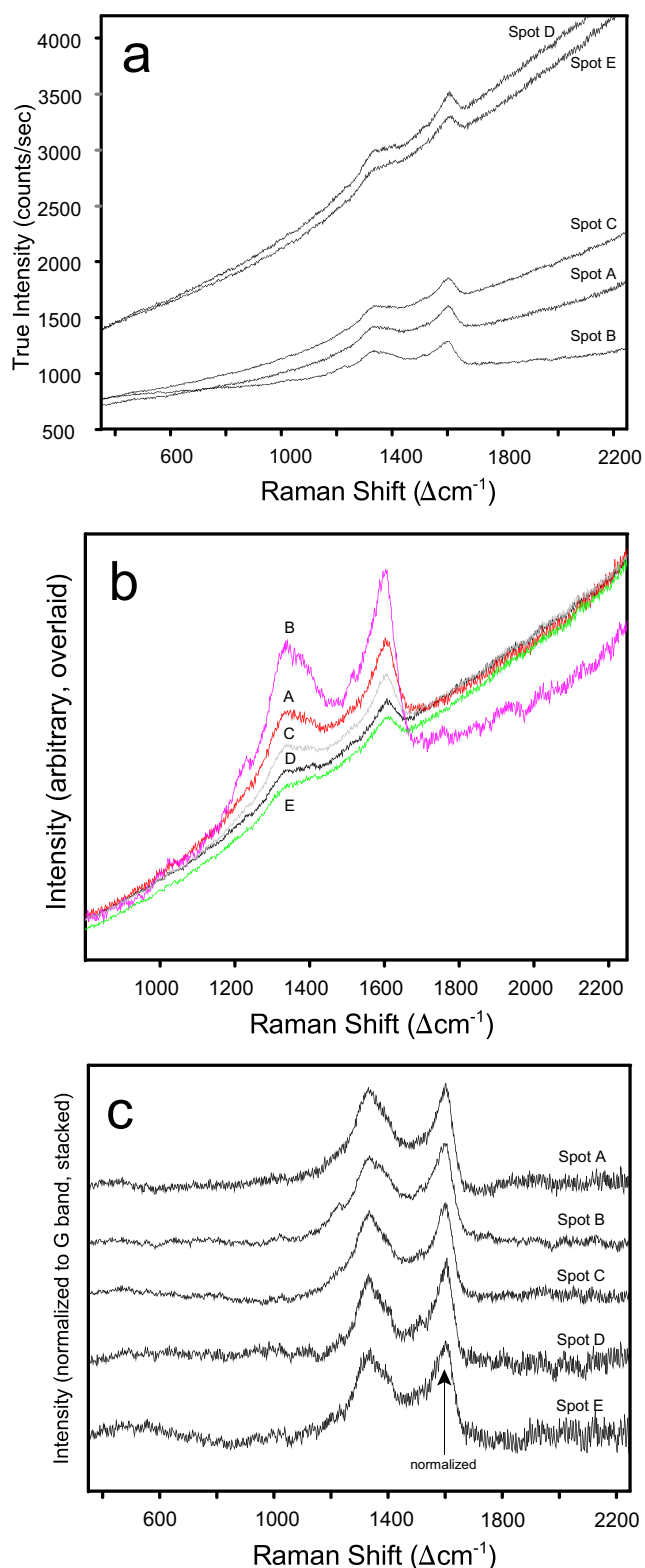


Fig. 4. Effect of baseline correction on the spectra (shown here for the low wavenumber region only) for the five spots of Stardust particle C2054,0,35,91,0 that show the presence of amorphous sp^2 -bonded carbon. For location of spots A–E, see Fig. 3. a) Spectra are plotted in true intensity units of counts per second. The spectrum for each spot shows the presence of amorphous carbon, but the amount of fluorescence is different in different fragments (spots) of the particle. b) Raw spectra are overlaid and displayed on an arbitrary scale (i.e., to full scale in the spectral window shown). c) Spectra shown in (a) were baseline-corrected and normalized to the intensity of the G band at $\sim 1600 \Delta\text{cm}^{-1}$. The normalized spectra are shifted along the y -axis (i.e., stacked) for better display. Only once the baseline correction is performed (i.e., the steep background is subtracted), and the spectra are normalized to the intensity of the G band at $\sim 1600 \Delta\text{cm}^{-1}$, does it become obvious that the Raman spectra obtained on the five different spots of this Stardust particle are indeed all identical (or at least very similar!).

stretching region, and (4) spectra from the light (colorless) looking areas (spots F and G) have abundant peaks (at both low and high wavenumbers) that are probably exclusively related to the presence of aerogel. Those spectra of spots F and G do not have the typical broad peaks for sp^2 -bonded carbon in the 1300–1600 Δcm^{-1} region, but they have several other fairly broad, and fairly strong bands in that spectral region. Those bands are at ~ 1300 , 1444, and 1604 Δcm^{-1} , and they are assigned to various C=C stretching modes of hydrocarbons that are most likely intrinsic organic contaminants of the silica aerogel capture medium (see below for more detailed presentations and discussions of spectra).

Stardust Sample C2092,6,80,51,0

After being pressed into Au, the particle (and the aerogel which came along with it) spread out on the Au foil over an area of roughly $\sim 100 \times \sim 100 \mu\text{m}$ (Fig. 2). There were two larger subgrains (the biggest one $< 10 \times < 4 \mu\text{m}$) and several much smaller fragments. The two largest subgrains were studied in detail and about 10 other micrometer-spots on much smaller remnants of particles were also analyzed. The individual small remnants of the original sample were recognized by their dark/black color and they were in the vicinity of the two largest fragments. Figure 5 shows the Raman spectra of five representative analyzed spots (spots α – ϵ , as indicated with circles). Spots α , β , γ , and ϵ were on dark areas (i.e., fragments of the actual particle), whereas spot δ was in the middle of the pressed-in largest fragment, and appeared colorless in reflected light. As was observed for the other Stardust grain (C2054, 0,35,91,0; see Fig. 3), also the spectra obtained on this Au mount away from any particle fragments showed no

“double-hump” characteristic for amorphous sp^2 -bonded carbon, (3) all spectra (with exception of the Au background, i.e., spot H) have peaks in the C-H

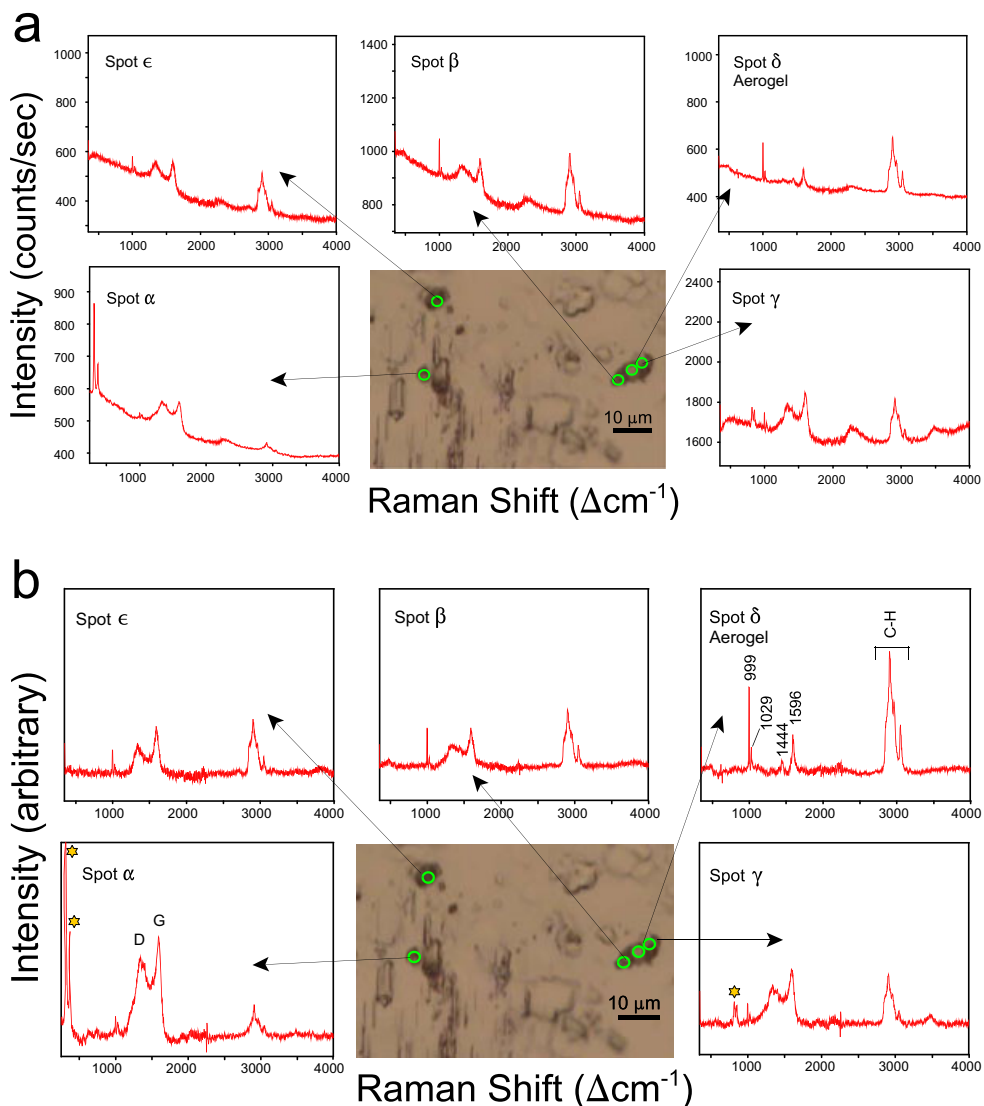


Fig. 5. Full Raman spectra ($350\text{--}4000\ \Delta\text{cm}^{-1}$) of five selected micrometer-sized spots of Stardust particle C2092,6,80,51,0 pressed into Au. The particle is seen in the Raman microprobe as a rotated (by $\sim 90^\circ$) mirror image compared to the way it is shown in Fig. 2. a) Raw spectra without any background correction or any other spectral manipulation. Note that the raw spectra of this particle look very different compared to the ones of particle C2054,0,35,91,0 (Fig. 3a), because here the Raman peaks are not superimposed on a very strong fluorescence background. b) Baseline-corrected spectra. Peaks due to olivine (found in spot γ) and pyrrhotite (found in spot α) are marked with stars.

fluorescence and no Raman peaks (spectra not shown here). Of interest, however, is that the spectra of the particle fragments (and/or the aerogel associated with them) of this Stardust sample are rather flat, and do not show the very steeply increasing fluorescence background that was observed for the other Stardust particle C2054, 0,35,91,0 (compare Figs. 3a and 5a). But even for raw spectra with fairly constant background counts, it becomes easier to see the Raman bands and compare peaks of different spectra once the baseline correction is performed. The baseline-corrected full (i.e., from 350 to

$4000\ \Delta\text{cm}^{-1}$) Raman spectra are plotted with arbitrary choices for the intensities (Fig. 5b) and show the following: (1) the dark-colored (i.e., black) areas (all spots except spot δ) show the bands characteristic for amorphous sp^2 -bonded carbon; (2) in addition, all the spectra with sp^2 carbon also show strong bands in the $2900\ \Delta\text{cm}^{-1}$ region; (3) the same number of bands at the identical positions in the $2900\ \Delta\text{cm}^{-1}$ region also occur in the light-colored areas associated with the grain (e.g., in spot δ) that are presumably aerogel-only areas; (4) the aerogel-only area (spot δ) has also very strong

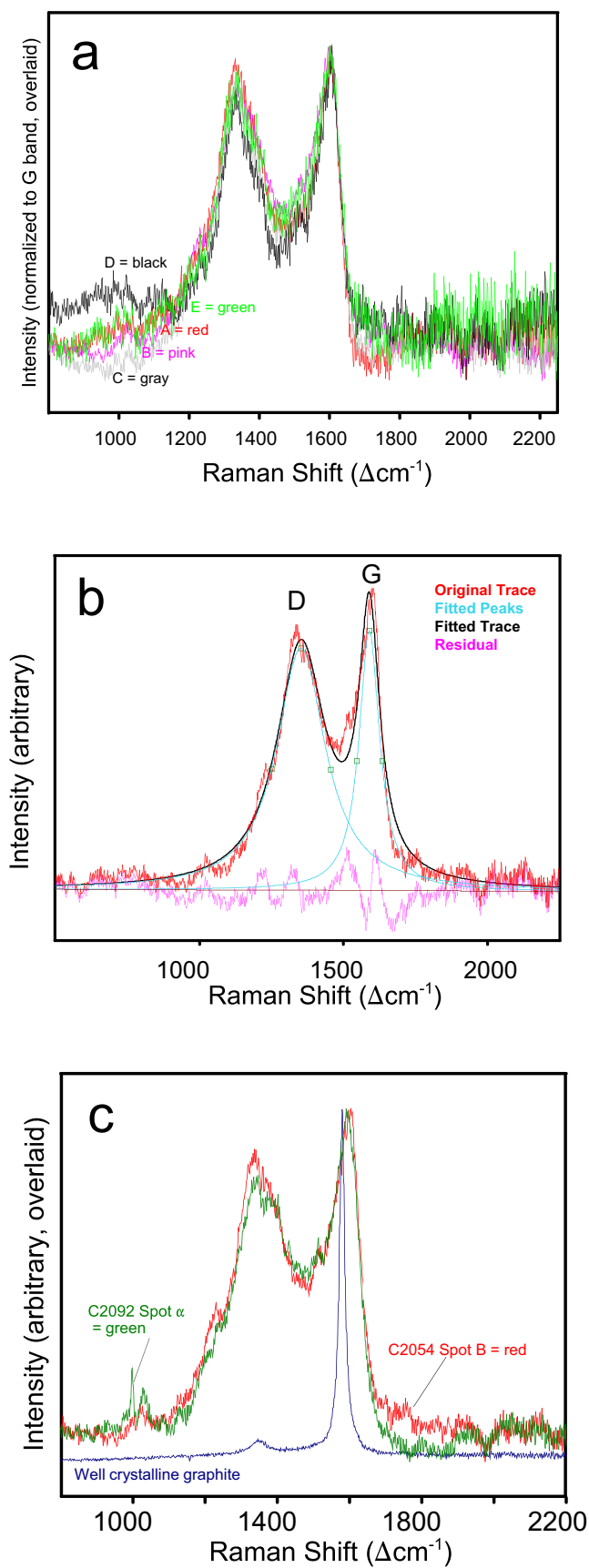


Fig. 6. a) Comparison of baseline-corrected Raman spectra for five different micrometer-sized spots of Stardust particle C2054,0,35,91,0. Spectra are normalized to G band at $\sim 1600 \Delta\text{cm}^{-1}$ and overlaid. b) Example of peak deconvolution of D and G bands due to sp^2 -bonded carbon in spot B of Stardust particle C2054,35,30; spectrum was deconvolved into two Lorentzian peaks; errors are fitting errors of individual spectrum: $D_{\text{position}} = 1352.5 \pm 0.2 \Delta\text{cm}^{-1}$; $D_{\text{width}} = 206.3 \pm 0.6 \text{ cm}^{-1}$; $G_{\text{position}} = 1589.9 \pm 0.1 \Delta\text{cm}^{-1}$; $G_{\text{width}} = 87.4 \pm 0.3 \text{ cm}^{-1}$; original baseline-corrected trace = red; calculated peaks = blue; fitted final trace = black; residual = pink. c) Comparison of Raman peaks caused by sp^2 -bonded carbon from fragments of two different Stardust particles from two different aerogel collector cells. Spot B is from Stardust particle C2054,35,30 (red trace), and spot α is from Stardust particle C2092,6,80,51,0 (green trace); Peaks at 999 and 1029 Δcm^{-1} are due to aerogel in cell C2092 (see also Figs. 8 and 9). Spectrum of graphite with a very small D (disorder) peak at $\sim 1350 \Delta\text{cm}^{-1}$ is shown for comparison.

peaks at 999, 1029, 1298 (small), 1444, and 1596 Δcm^{-1} ; (5) the peaks at 999 and 1029 Δcm^{-1} can be seen in all spectra obtained from this sample (except on the Au background); and (6) in addition to sp^2 -bonded carbon, also other species/minerals were detected in this sample (indicated with stars in Fig. 5b): Olivine (peaks at 820 and 853 Δcm^{-1}) was found on the upper end of the largest subparticle (spot γ), and pyrrhotite (strong peaks at 314 and 372 Δcm^{-1}) was detected in spot α . (See below for more detailed presentation of spectra and discussion of specific peak positions.)

Comparison of Baseline-Corrected Spectra

All dark looking spots analyzed in the two Stardust particles of this study (i.e., the actual fragments of the Stardust grains rather than the aerogel from the capture cells) have the broad “double-hump feature” characteristic for amorphous sp^2 -bonded carbon (D and G bands). These peaks are easy to detect with Raman spectroscopy, and they are often the only peaks that can be detected in materials that contain sp^2 -bonded carbonaceous materials. The overall characteristics of the D and G bands are very similar within a given particle (see Fig. 4c). Figure 6a shows baseline-corrected Raman spectra for five different micrometer-sized spots of particle C2054,0,35,91,0. The mean ($n = 5$) of the Lorentzian peak deconvolution results of the D and G bands (two-band fit) for the spectra of Stardust particle C2054,0,35,91,0 (spots A through E; overlaid in Fig. 6a) are $D_{\text{position}} = 1347.4 \pm 3.3 \Delta\text{cm}^{-1}$, $D_{\text{width}} = 170.6 \pm 28.4 \text{ cm}^{-1}$, $G_{\text{position}} = 1592.6 \pm 2.2 \Delta\text{cm}^{-1}$, and $G_{\text{width}} = 77.5 \pm 8.3 \text{ cm}^{-1}$. Figure 6b shows the results for the peak deconvolution for an individual spectrum (spot B) as an example. These quantitative parameters

are in general agreement with previously reported results for Stardust particles (e.g., Sandford et al. 2006; Muñoz-Caro et al. 2008; Rotundi et al. 2008), but the deconvolved D_{widths} of the spectra in the present study are narrower than the ones reported previously (e.g., the latter ranged from 204.4 ± 16.8 to $392 \pm 12 \text{ cm}^{-1}$ in a study of 13 different particles obtained by five different laboratories; Rotundi et al. 2008). Whereas the peaks due to the amorphous sp^2 -bonded carbon are essentially overlapping for all the fragments of particle C2054, 0,35,91,0 (Fig. 6a), there are some small differences among the spectra of different fragments for particle C2092,6,80,51,0 (spectra not shown). Overall, however, the characteristics of the D and G bands are quite similar for both of the studied particles (see examples of two overlaid spectra in Fig. 6c). The detailed analysis and discussion of the quantitative Raman spectral parameters of the amorphous sp^2 -bonded carbon bands and their comparison to data obtained on meteorites and IDPs, however, are not the subject of this study, but will be presented in a different paper (Wopenka, in preparation). Rather, the focus of this study is on those Raman bands that were detected in Stardust particles *in addition* to the strong (and always present) D and G bands.

Figure 7 investigates in more detail the bands found in the light-colored spots G and F of particle C2054,0,35,91,0, and compares them to the ones found in dark-colored spot B. Note that the baseline-corrected spectrum of spot B not only shows the D and G bands but also very prominent peaks in the 2900 cm^{-1} region. The spectra of spots G and F are likely to be the spectra of aerogel only (because they have no D and G bands) and have peaks at $1298, 1444, 1604 \text{ cm}^{-1}$ and at $2850, 2908, 2965 \text{ cm}^{-1}$. The positions of these peaks are indicated by vertical lines in Fig. 7. The three high wave number peaks in the C-H stretching region are exactly at the same positions in the spectra of the dark spots (A–E; only spectrum for B is shown in Fig. 7). The peaks in the $1300\text{--}1600 \text{ cm}^{-1}$ region, however, are difficult to detect in any spectrum that also shows the (always strong) sp^2 -bonded carbon peaks. Spot B is the only dark particle fragment that showed some small peaks at lower wave numbers (at 1232 and 1511 cm^{-1} , indicated by stars in Fig. 7a) superimposed on the D and G bands. These peak positions, however, are different from the ones found in spots G and F, and thus might be unrelated to the peaks caused by the contaminating aerogel.

Figure 8 investigates in more detail the spectra of two of the spots (β and γ) that show sp^2 -bonded carbon bands in the other particle (C2092,6,80,51,0). Those spectra are compared to the spectrum of spot δ , which (presumably) is the result of aerogel only (because it does not have D and G bands). Please note that the spectra

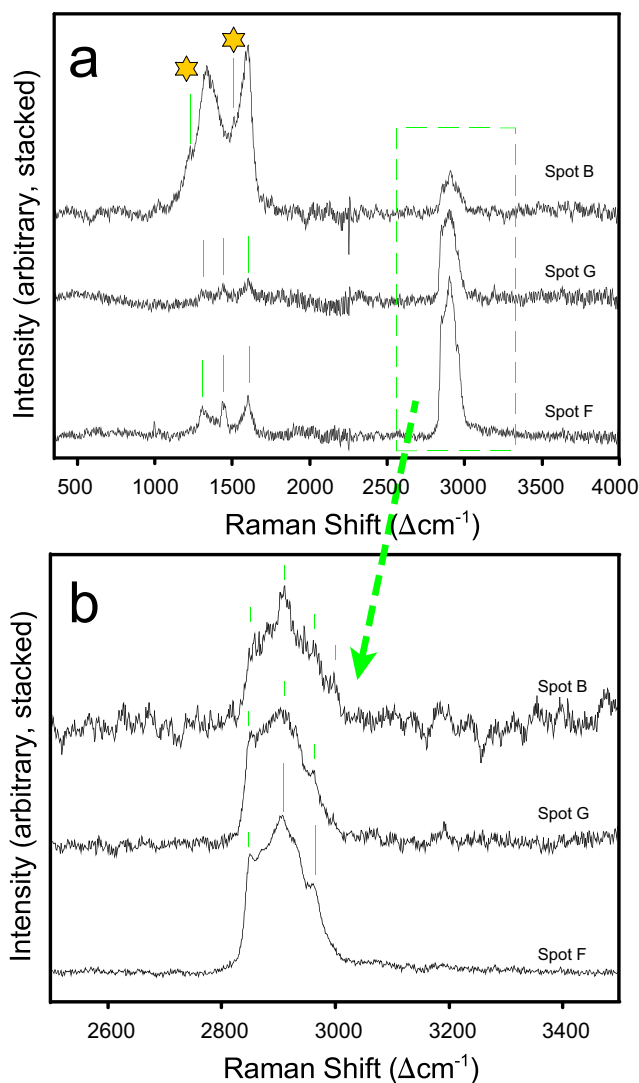
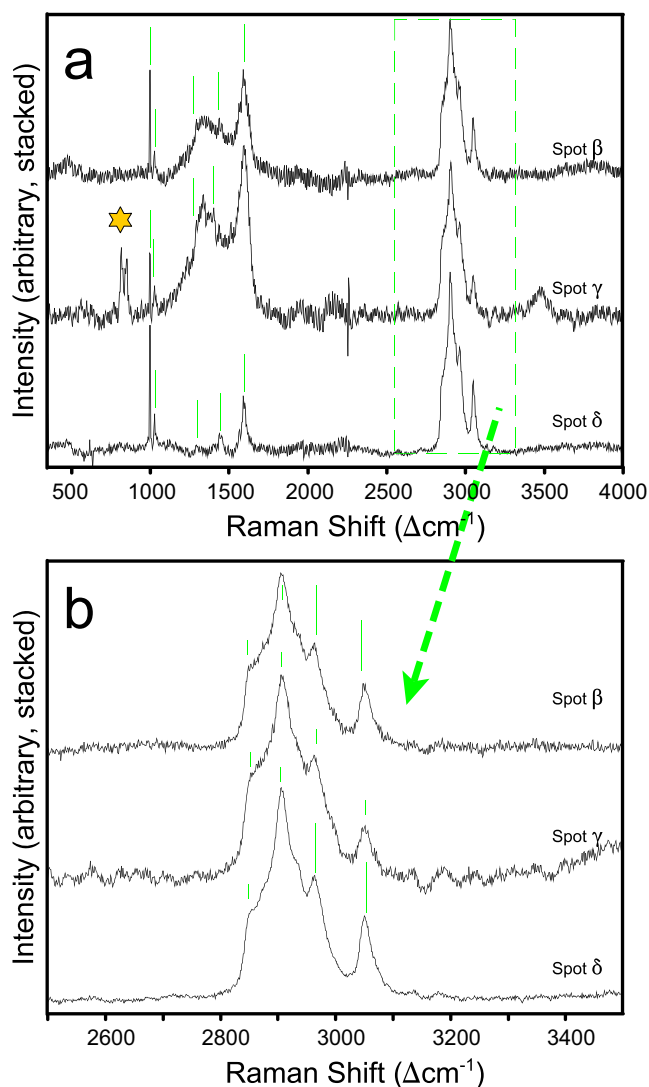


Fig. 7. Comparison of baseline-corrected spectra with and without amorphous sp^2 -bonded carbon obtained of different micrometer-sized spots of Stardust particle C2054,0,35,91,0. Peaks marked with vertical lines are discussed in text. a) Spectrum of spot B is selected for comparison to the spectra of spots F and G, which are presumably aerogel-only spectra. Peaks marked with stars were only found in spot B (see text). b) Zoom-in to C-H stretching region shows that peaks observed in spot B are at exactly the same position as the ones found in (presumably) aerogel-only spectra.

for spots $\alpha, \beta, \gamma,$ and ϵ (spectra for β, γ are shown in Fig. 8a) not only show the sp^2 carbon bands but also very strong bands at 999 and 1029 cm^{-1} , and at $2850, 2908, 2965,$ and 3050 cm^{-1} . All those peaks (with the exception of the D and G bands) also occur in the spectrum of spot δ that is (presumably) the one of aerogel only. In addition, several peaks in the $1300\text{--}1600 \text{ cm}^{-1}$ region can be seen in the spectrum for spot δ (Fig. 8a). Those peaks occur at $1298, \sim 1444,$ and



strong bands at the following wavenumbers: 2850 cm^{-1} (symmetric CH_2 stretch), 2908 cm^{-1} (asymmetric CH_2 stretch), and 2965 cm^{-1} (antisymmetric CH_3 stretch), all of which are typical for alkanes. These three C-H stretch bands with similar relative intensity ratios were found in the spectra of all the Stardust fragments of this study. Thus, I conclude that any peaks observed in the C-H stretch spectral region found in the spectra of Stardust particle fragments are due to aerogel only. It is my opinion that those peaks that were found in each single spectrum taken during the course of this study must be due to contamination with aerogel and are not inherent to the extraterrestrial material.

In addition to the C-H stretch bands typical for alkanes, aerogels from both cells have bands at 1298 cm^{-1} (could be CH_2 twist), 1444 cm^{-1} (could be $\text{N}=\text{N}$ stretch), and $\sim 1600 \text{ cm}^{-1}$ ($\text{C}=\text{C}$ stretch). These aerogel bands in the $1300\text{--}1600 \text{ cm}^{-1}$ region clearly overlap with the sp^2 carbon bands of the amorphous carbon in the spectra of the grain fragments. Specifically, the fairly strong pointed bands at 1596 and 1604 cm^{-1} (in the aerogel of the C2092 and C2054 collection cell, respectively; see Fig. 9b) may influence the intensity and position of the G band of the sp^2 -bonded carbon feature that is present in all grain spectra. Therefore, any peak deconvolution and quantitative interpretation of the sp^2 carbon band parameters (i.e., peak widths and positions of both the D and G bands) in aerogel-contaminated Stardust particles need to be interpreted with caution.

In addition to the bands in the C-H stretch region and the ones in the $1300\text{--}1600 \text{ cm}^{-1}$ region (which occur in the aerogel of both collector cells), the aerogel of cell C2092 also showed strong bands at the following wavenumbers (Fig. 9b): 3050 cm^{-1} (probably due to aromatic C-H stretch of alkyl benzene), 1029 and 999 cm^{-1} (can be both due to ring “breathing” of benzene rings). Thus, it seems that the aerogel of cell C2092 carries some aromatic contamination in addition to the aliphatic contamination that is seen in the aerogel of both collector cells.

It is well recognized that the aerogel used as capture medium for the Stardust mission was not clean and contamination-free, and up to 9 wt% carbon was found in the SiO_2 aerogel (Gallien et al. 2008; Zolensky et al. 2008). This organic preflight contamination of the aerogel collection material was not recognized prior to sending the collectors to space. Contamination with organic carbon-containing aerogel was addressed postflight, and has been documented in Stardust particles with the use of various analytical techniques (e.g., Sandford et al. 2010; De Gregorio et al. 2011), but was not yet addressed in any detail in a Raman spectroscopic study. Unfortunately, however, based on the findings of this study it is concluded that the organic contamination

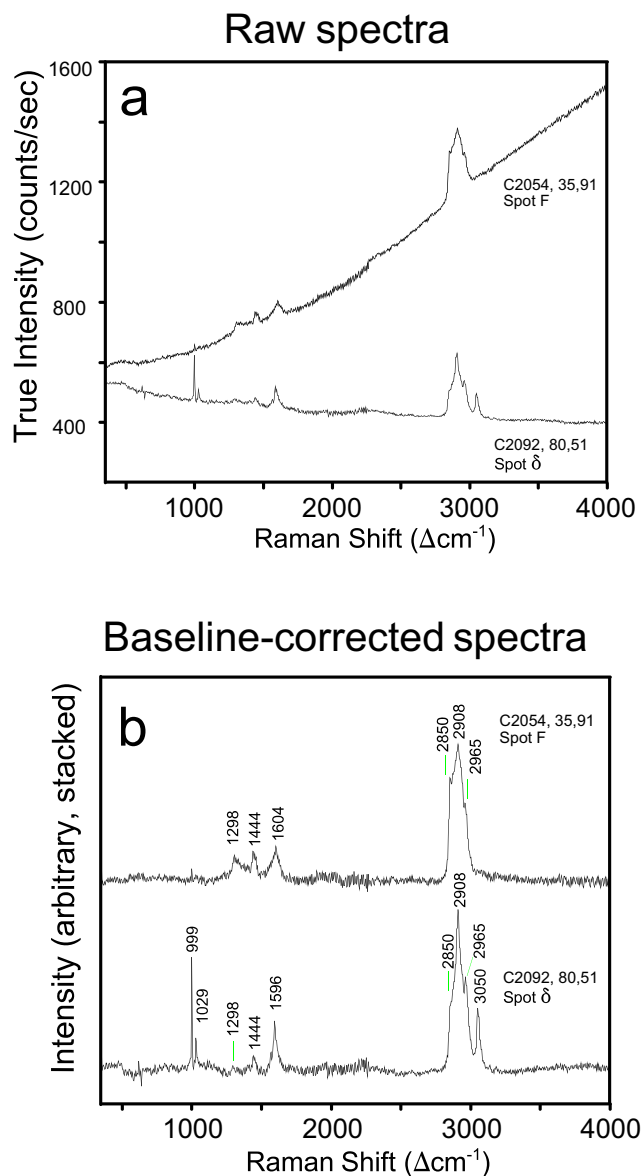


Fig. 9. Comparison of raw and baseline-corrected, normalized Raman spectra of aerogel associated with two different Stardust particles. a) Raw spectra without any background correction or any other spectral manipulation; spectra are plotted in true intensity units of counts per second. b) Spectra shown in (a) were baseline-corrected and normalized to the intensity of the band at $\sim 2908 \text{ cm}^{-1}$. The normalized spectra are shifted along the y-axis (i.e., stacked) for better display.

of the preflight aerogel will make the Raman-based interpretation of certain organics (e.g., the ones with aliphatic CH_3 groups) found in returned samples impossible. Vibrational frequencies in organic molecules are typically true fingerprints in that they are very characteristic of the chemical bonds (or group of bonds) in a specific molecule. Raman spectra are typically

sensitive to details in the structure and to the local environment of an organic molecule. This means that spectra of organics are sensitive not only to the functional group (e.g., methyl) but also to the molecular structure this functional group is connected to. With one single exception in the spectra of one single location (spot B in particle from C2054, see Fig. 7a and discussion below), the organic bands found in the fragments of the Stardust particles of this study are identical (in all aspects: number of peaks, positions of peaks, relative peak intensities) to the organic bands found in the aerogel of their respective collector cell. The only possibility that intrinsic organics were present in the extraterrestrial material would be if the Stardust-related organics (in the two particles subjected to this study) are identical in nature, composition, and abundance to the contamination-related organics. I consider this possibility highly unlikely. The one and only exceptional result was the one obtained for spot B of sample C2054,0,35,91,0. Spectra obtained in this spot show faint peaks at 1232 and 1511 Δcm^{-1} that are superimposed on the strong D and G bands (see Fig. 7a). The positions of these bands differ from those that were detected in the aerogel associated with this particle. Thus, these bands could be related to some organics that are intrinsic to the extraterrestrial particle, but they could not be assigned to specific functional groups or bonds.

Differences Between Aerogel Spectra From Different Aerogel Collector Cells

The most striking (and to me unexpected) differences that were observed between the spectra obtained from the particles in the two different collector cells are related to the nature/chemistry of the silicon aerogel. Figure 9a shows the raw spectra of the aerogel associated with the two Stardust samples side by side. All the spectra for the grain that came from aerogel cell C2054 show strong fluorescence, whereas all the spectra for the grain that came from cell C2092 are flat (compare raw spectra in Figs. 3 and 5). The Au mounting substrate does not show any fluorescence (see spot H in Fig. 3), but the light-colored areas of sample C2054,0,35,91,0 (spots F and G, see Fig. 3), which are presumably aerogel only (without any intermixing with Stardust grain fragments) show a strong steep fluorescence background on which the aerogel-related Raman peaks are superimposed. Thus, it can be concluded that the fluorescence is related to the properties/chemistry of the aerogel. Given that there is a very intimate relationship of the Stardust grain with the aerogel, it is impossible to obtain a Raman spectrum of the grain only. Therefore, it has to be expected that the raw spectra of the grain fragments all show the same strong increasing underlying background

as the aerogel-only spectra, which is indeed the case (Fig. 3).

By contrast, spectra of the aerogel-only areas of sample C2092,6,80,51,0 also have plenty of Raman peaks, but they are sitting on a rather flat (or even decreasing) overall background across the full spectral range (see spectrum of spot δ in Fig. 5). Similar to the sample from cell C2054, the raw spectra of the actual sample from cell C2092 have the same overall background characteristics as the spectra of its associated aerogel. In other words, if the aerogel-only spots show fluorescence, then all spectra of the actual grain fragments also show fluorescence (the case for sample from cell C2054), and if the aerogel-only spots have a flat background across the spectral range, then the grain spectra have a flat background (the case for sample from cell C2092). This consistent and systematic finding for all the spectra obtained of the two Stardust samples (i.e., not only the spectra shown in Figs. 3 and 5 as examples) confirms that the aerogel associated with the two particles (or the two tracks?) was inherently different.

In terms of the actual Raman bands, the aerogels from the two collector cells were not identical either. This can be best seen in a comparisons of their baseline-corrected spectra: both the stacked and overlaid display of the spectra show that the Raman bands at 999, 1029, and 3050 Δcm^{-1} are only present in the spectra associated with cell C2092 (Figs. 9b and 10). Although the peaks at 2850, 2908, and 2965 Δcm^{-1} occur in both types of aerogel spectra, their relative intensities are different (Fig. 10b), which is another proof of inherent differences in the aerogel of the two collector cells, at least as it was in association with the two Stardust particles that I received from NASA for analysis.

In summary, the degree of fluorescence as well as the exact Raman peak positions and relative intensities of the bands in the C-H stretch region that are associated with aerogel contamination are distinctly different for the two particles. Of further interest is that two other Stardust particles that were previously studied in the same laboratory at Washington University in St. Louis have yet two different types of fingerprints in the C-H stretching region (Fig. 11). Particle C2054,0,35,30 was studied during the Preliminary Examination Team (PET) Phase (Rotundi et al. 2008), and although it originated from the same aerogel cell (C2054) and the same impact particle (#35), it did not have the same spectral features as C2054,0,35,91 that was the subject of this study. Even more interesting is the fact that different fragments of the same particle (i.e., C2054,0,35,30 from the PET study) showed different types of C-H stretching modes. One type of spectrum that was associated with this PET grain is included as spectrum d in Fig. 11, another one is shown in the PET collaboration results (Rotundi et al.

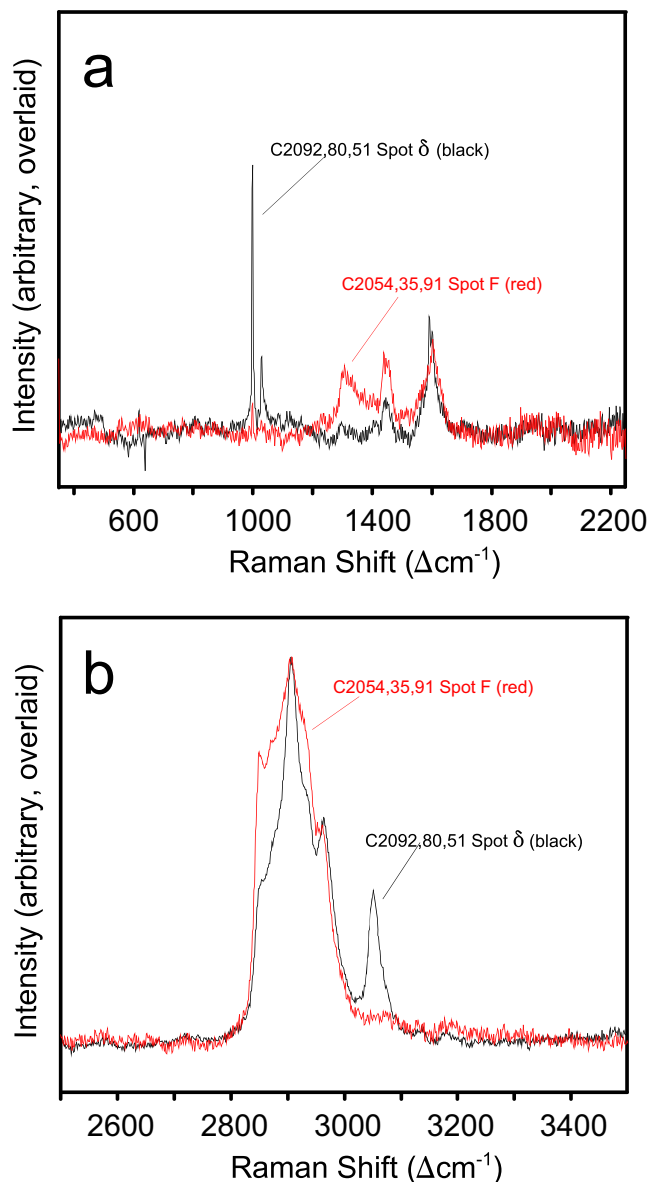


Fig. 10. Comparison of baseline-corrected Raman spectra (intensity normalized to 2908 cm^{-1} band) of the aerogel associated with two different Stardust particles (see Fig. 9b for the exact peak positions of the aerogel spectra from the two collector cells). a) Low wavenumber region that overlaps with sp^2 -carbon bands (which are present in all particle fragments); peaks at 999 and 1029 cm^{-1} only occur in aerogel spectrum from cell C2092. b) High wavenumber region (C-H stretching modes); band at 3050 cm^{-1} only occurs in aerogel spectrum from cell C2092.

2008; spectrum 1 in their Fig. 6b). The latter spectrum (not shown here) had exactly the same peaks that were also found during a detailed Raman analytical study of Stardust sample Al-foil C2125W1 (Wopenka, unpublished data) with a prominent peak at 2881 cm^{-1} , which is shown as spectrum c in Fig. 11.

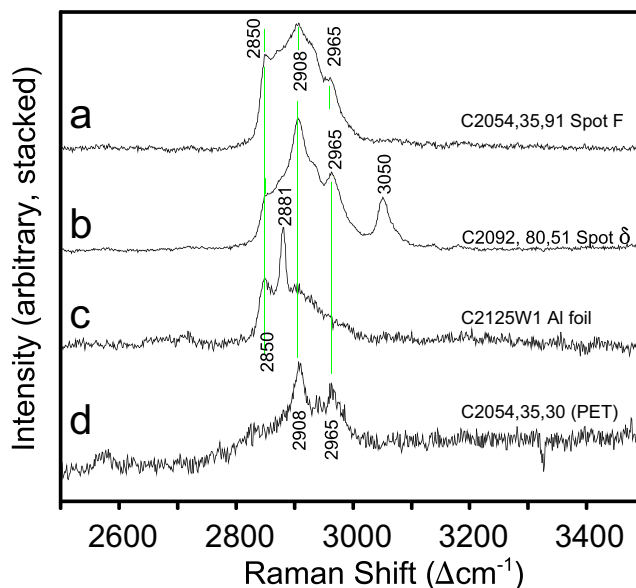


Fig. 11. Comparison of Raman bands in C-H stretch region detected during the analyses of four different Stardust samples analyzed at Washington University in St. Louis. a) Particle C2054,0,35,91,0 from present study (contaminated with aerogel from the capture cell). b) Particle C2092,6,80,51,0 from present study (contaminated with aerogel from the capture cell). c) Material analyzed from wall of crater on Al-foil C2125W1. d) Particle C2054,35,30 that was studied during the efforts of the Preliminary Examination Team (Rotundi et al. 2008).

Of further note is that yet another Stardust particle (terminal particle “Ada” from track #26) from the same aerogel cell (C2054) whose Raman spectrum was previously documented (Wopenka et al. 2008) showed the same aerogel-related peaks that were found for cell C2054 in the present work (Fig. 9). Although in the past we were able to rule out that the Raman peaks found for Ada were not related to the acrylic embedding medium, we previously were not able to assign the peaks found for Ada exclusively to aerogel contamination, and thus we had left open the possibility that the peaks reported for Ada originated from the extraterrestrial material (Wopenka et al. 2008). Only in retrospect does it become obvious that the Raman peaks documented for Ada are exactly the ones characteristic for the aerogel of collection cell C2054. All of the bands in the C-H stretch region (examples shown Fig. 11) are consistent with the presence of alkane-type saturated hydrocarbons (as discussed in detail in Rotundi et al. 2008), and based on the findings in this study they are related to the aerogel collection medium (and thus unlikely to be inherent to the particles). What remains unclear is why there are so many different kinds of spectral signatures that can be detected in the C-H stretch region. This either means that the specific properties of aerogel (its treatment before and/or after synthesis, the temperature it experienced, the

effect of individual particle impacts, etc.?) were different for samples that were analyzed from the same collection cell (and even the same track: C2054,35,30 during PET phase and C2054,35,91 in this study), or that the C-H stretch peaks are caused (at least in part) by cometary materials after all. Given that even different spots in the same particle (C2054,35,30 from PET study) can have different peaks in the C-H region makes the situation even more complicated and puzzling.

Of further note is that no Raman peaks in the C-H stretch region were detected for terminal Stardust particle “Febo” C2009,2,57 (Matrajt et al. 2008) that was also previously studied with the same high-sensitivity Raman spectrometer (Wopenka, unpublished results) as the Au-mounted particles discussed in the present work. The reason that no aerogel-related Raman peaks in Febo were detected could be related to the specific sample preparation of Febo; the Raman study of Febo was done on a microtomed thin-section (but so was the one on Ada!) that exposed the interior of the grain to Raman analysis (see more related discussion below).

Olivine and Sulfide in Stardust Detected via Raman Spectroscopy

As mentioned before, the spectra of every single particle fragment of this Raman study show the very dominant sp^2 -bonded carbon double-peak that is characteristic for either amorphous elemental carbon or hydrogenated aromatic macromolecular carbon (e.g., large polycyclic aromatic hydrocarbons [PAHs]). But in addition to this strong, always present sp^2 -bonded carbon feature (and, of course, the always present aerogel peaks), two of the fragments of Stardust sample C2092,6,80,51,0 also showed peaks characteristic of sulfide and olivine (Fig. 12). The strong peaks due to sulfide are at 314 and 372 Δcm^{-1} and indicate the presence of the mineral pyrrhotite, and the peaks for the characteristic olivine doublet are at 820 and 853 Δcm^{-1} .

Raman peaks below 1200 Δcm^{-1} for inorganic covalently bonded minerals are extremely difficult to detect in the presence of nongraphitic sp^2 -bonded carbon. This is due to the fact that the experimental Raman scattering efficiencies of nongraphitic sp^2 -bonded C-C vibrations are substantially higher than the scattering efficiencies associated with the bonds that occur in most silicates, oxides, sulfides, and other minerals. This means that the peaks caused by the sp^2 -bonded C-C vibrations of the carbonaceous material always will dominate the spectrum (or at least be very strong), even if the major components of the sample are noncarbonaceous. In fact, even an extremely small concentration of sp^2 -bonded carbonaceous material (e.g., amorphous elemental carbon, large PAHs, and/or macromolecular PAH-like

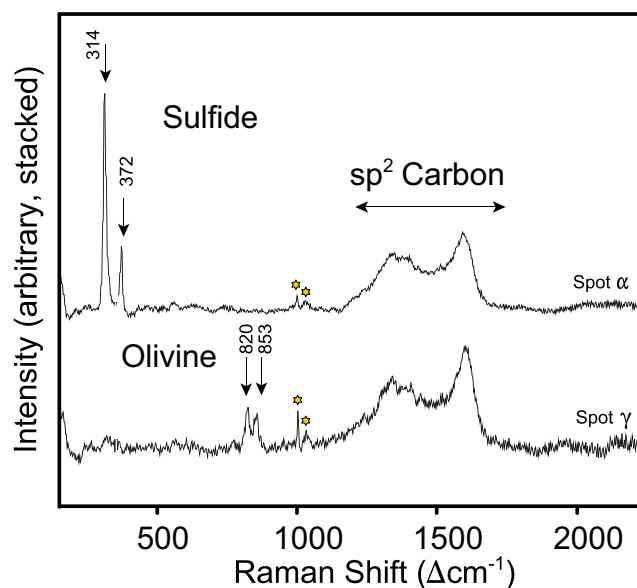


Fig. 12. Raman spectra of two fragments of Stardust particle C2092,6,80,51,0, which show not only peaks for sp^2 -bonded carbon but also peaks for the sulfide pyrrhotite (spot α) and olivine (spot γ). Bands due to aerogel are marked with a star.

molecules) on or below the particle surface typically prevents the Raman detection of other minerals in IDPs and Stardust particles. At least this is the case for “bulk” micrometer-sized particles that are mounted, crushed, and pressed into Au as mounting medium, which was the sample preparation for the particles in this study. Similar sample preparation methods were also used in several previous Raman studies of IDPs and Stardust particles (Wopenka 1988; Quirico et al. 2005; Muñoz-Caro et al. 2006; Sandford et al. 2006; Rotundi et al. 2008; Busemann et al. 2009), and none of these studies revealed the presence of any minerals (sulfides, silicates, and others) in addition to the detected sp^2 -bonded carbon. Thus, the detection of olivine and pyrrhotite via Raman spectroscopy in the Au-mounted Stardust particles of this study is an unusual finding, although the presence of these (and other) minerals in returned cometary material is of course well established from the use of other analytical techniques.

However, a different (more complicated) kind of sample preparation exposes the interior of a particle and makes it accessible to Raman analysis, and this might make it easier to detect minerals in the presence of sp^2 -bonded carbon. Matrajt and Brownlee (2006) developed a sample preparation technique that involves mounting the Stardust particle in an acrylic resin, and this mount is then ultramicrotomed into 50–90 nm thick slices. Each ultramicrotomed section contains a slice of the particle and surrounding aerogel (and the acrylic resin, of course), and is placed on a Cu or Au TEM grid for

further analysis (Matrajt et al. 2008). It has previously been shown that such 80 nm thick slices of a Stardust particle (terminal particle “Febo” C2009,2,57) that were deposited on an Ni-grid (to avoid sample heating) could be successfully Raman analyzed (Wopenka et al. 2007). The slicing (microtoming) revealed the interior of the Stardust particle Febo to Raman analysis, and thus increased the probability of detecting Raman signals from (potentially present) additional minerals, despite the presence of the strong (and usually everything else overwhelming) peaks for nongraphitic sp^2 -bonded carbon. And indeed, pyrrhotite could be successfully identified in Stardust particle Febo via Raman spectroscopy (Wopenka et al. 2007), and thus the previously obtained Raman spectra for cometary pyrrhotite can be compared to the ones found in the Stardust particle of this study (C2092,6,80,51,0).

The Raman spectrum for spot α (Figs. 5 and 12) has strong peaks at 314 and 372 Δcm^{-1} . Such strong peaks at low wavenumbers are typical for iron-bearing sulfides. The exact peak positions listed in the literature (and found on natural sulfide mineral samples), however, are not always exactly the same for a given mineral. For instance, Pasteris (1998) lists the peaks for pyrite (FeS_2) at 342 and 378 Δcm^{-1} , and for marcasite (FeS_2) at 324 Δcm^{-1} and a smaller doublet at 393 and 406 Δcm^{-1} . Mernagh and Trudu (1993) list the peaks for pyrite at 342 and 377 Δcm^{-1} and the ones for marcasite at 324 and 387 Δcm^{-1} . The peaks in spot α are not consistent with either of those FeS polymorphs, and are rather most likely caused by the nonstoichiometric iron sulfide pyrrhotite (Fe_{1-x}S). Especially for pyrrhotite (but also for other sulfides), the exact peak positions can vary substantially as a function of its nonstoichiometric composition. The “ruff database” lists Raman spectra of minerals on the internet (<http://www.ruff.info>) and shows the peaks for a pyrrhotite sample to be at 338 and 371 Δcm^{-1} , whereas Wang et al. (2004) have reported spectra for two different pyrrhotites (with unknown exact stoichiometry) that have different exact peak positions, but for both samples the lower peak of the sulfide doublet is close to 300 Δcm^{-1} . To add to the confusion, Steele et al. (2006) mapped a Raman peak in carbonate globules from the meteorite Allan Hills 84001 that occurs at 215 Δcm^{-1} , and which they claim to be caused by pyrrhotite. In summary, the exact Raman peak positions for pyrrhotite can vary as a function of stoichiometry as well as with the degree of ordering, and reflect variations in the Fe-S bond lengths. But all pyrrhotites will have two strong Raman peaks close together below 400 Δcm^{-1} .

As mentioned above, pyrrhotite was previously detected via Raman spectroscopy in another Stardust particle named “Febo” (Wopenka et al. 2007), and

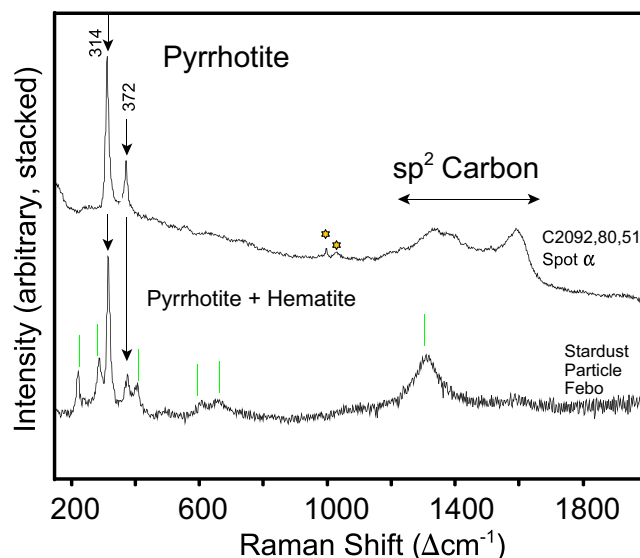


Fig. 13. Comparison of Raman spectra obtained on two different Stardust particles in which pyrrhotite could be identified (marked with arrows). Top: Spectrum of spot α of Stardust particle C2092,6,80,51,0 also shows strong D and G carbon bands. Peaks marked with a star at 999 and 1029 Δcm^{-1} are caused by aerogel contamination. Bottom: Pyrrhotite detected in spectrum of large sulfide area of terminal Stardust particle Febo (Wopenka et al. 2007). Bands marked with green lines are at 225, 292, 408, 610, 660, and 1319 Δcm^{-1} , and are assigned to hematite ($\alpha\text{-Fe}_2\text{O}_3$) (see text for discussion).

Fig. 13 compares the pyrrhotite spectrum obtained on a fragment (spot α) of grain C2092,6,80,51,0 pressed into an Au substrate with the one obtained on a 80 nm microtomed thin-section of the particle Febo. The sulfide peak positions for Febo are at 317 and 375 Δcm^{-1} (marked with arrows in Fig. 13), i.e., are very close to the ones obtained for the particle of the present work (at 314 and 375 Δcm^{-1}). This indicates that the pyrrhotite compositions of the two different Stardust samples must be very similar, although the particles came from different impact tracks, with Febo being a terminal particle and the other one from the side wall of a bulbous track. Note that the spectrum of Febo also shows the Raman peaks for hematite ($\alpha\text{-Fe}_2\text{O}_3$) at 225, 292, 408, 610, 660 Δcm^{-1} , as well as a strong wide resonance peak that occurs at 1319 Δcm^{-1} when the 532 nm wavelength is used for excitation of the Raman effect. However, the presence of hematite may or may not be the result of sulfide oxidation during Raman analysis. In other words, the detection of hematite in Febo might be due to an analytical artifact, and thus it is not unambiguously established that the Raman-detected hematite is indigenous to the extraterrestrial material and/or was created during the impact.

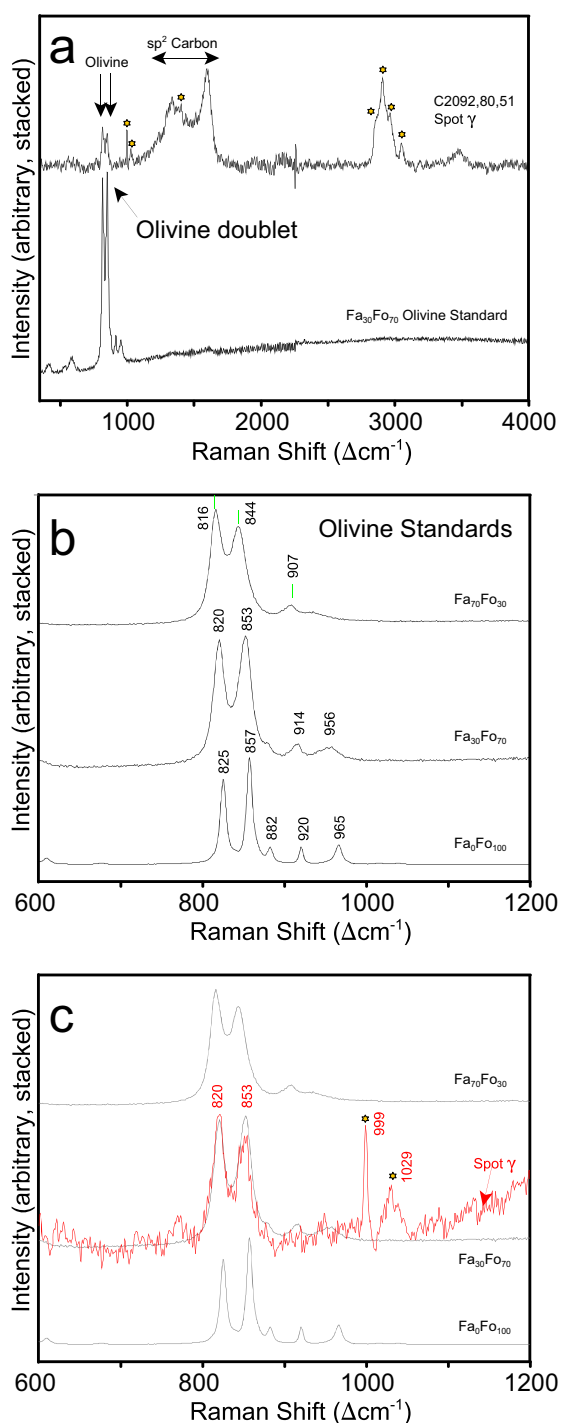


Fig. 14. Raman spectrum of spot γ in Stardust particle C2092,6,80,51,0 compared to spectra for olivine standards of different composition. a) Comparison of full Raman spectra (350–4000 Δcm^{-1}). Note that the Stardust sample also has the peaks for amorphous sp^2 -bonded carbon and the peaks due to the aerogel contamination (marked with stars). b) Spectral range of 600–1200 Δcm^{-1} that shows the exact peak positions for olivines with different compositions. Synthetic standard samples were provided by D. Dyar. c) Stardust spectrum of spot γ (in red) overlaid on olivine standard spectrum, which shows that the composition of olivine in this Stardust particle is $\text{Fa}_{30}\text{Fo}_{70}$.

A previous Raman study of two Stardust particles (C2044,0,41,0,0 and C2005,2,121,0,2,0) also reported the detection of low wavenumber peaks characteristic for hematite (and for magnetite), and the presence of both iron oxides in the particles was confirmed with other instrumental analysis techniques (Bridges et al. 2010); however, their Raman spectra do not show the peaks for the D and G bands; thus the particles studied by Bridges et al. (2010) apparently either (1) did not contain any sp^2 -bonded carbonaceous materials that typically makes the Raman detection of the peaks for iron oxides (and other minerals) very difficult/impossible, or (2) they were prepared as thin-sections so that they could acquire spectra of the interior of the particles, and successfully identify those oxides in Stardust via Raman spectroscopy.

The Raman spectrum for spot γ in sample C2092,6,80,51,0 (Figs. 5 and 14) has peaks that can be assigned to the Si-O stretch vibrations in olivine. The peaks occur at 820 and 853 Δcm^{-1} and are known as the “olivine doublet.” The exact peak positions of both peaks in this doublet depend on the exact composition of the olivine. Because there is a monotonic shift in peak positions as a function of cation substitution between fayalite (Fe_2SiO_4) and forsterite (Mg_2SiO_4), the chemical composition of the olivine can be determined from the exact peak positions of the Si-O modes within the SiO_4 tetrahedra, i.e., the “olivine doublet” (Kuebler et al. 2006). Figure 14b shows the spectra (between 600 and 1200 Δcm^{-1}) of three different olivines that were obtained on a suite of synthetically produced olivine standards (the so-called “SUNY” olivines provided by Dyar; Dyar et al. 2009). The Raman peaks shift to lower wavenumbers with higher Fe content. Based on comparison to the spectra of synthetic olivines, the composition in the fragment of Stardust particle C2092, 6,80,51,0 can be determined as $\text{Fa}_{30}\text{Fo}_{70}$ (Fig. 14c).

In summary, due to the strong absorption of the visible laser beam by the sp^2 -bonded carbon, as well as due to the extremely strong Raman scattering efficiency of amorphous sp^2 -bonded carbon (as already mentioned above), Raman analysis unfortunately is typically of only limited usefulness when it comes to finding out something about the mineralogy of other phases (such as silicates, oxides, or sulfides) of particles that are covered by carbonaceous material. For the excitation wavelengths most commonly used in Raman spectroscopy (488, 514, or 532 nm) the laser light will be totally absorbed in the top ~ 100 nm surface layer of the sample, and minerals/molecules/bonds below this layer cannot be detected. Therefore, for samples that contain such carbonaceous materials (even in minor amounts as coating), Raman spectroscopy will be a surface technique, and usually cannot give any information about the interior composition of the samples (unless the sample is prepared

as a microtomed thin-section). This is an essential handicap for carbonaceous samples, which are gray or black, and thus opaque to the human eye as well as to the monochromatic visible light that is used in most Raman spectroscopic instruments.

CONCLUDING REMARKS

Raman spectra obtained on the two Stardust particles analyzed in this study have many very distinct and strong bands at both low and high wavenumbers. All particle fragments showed the (always present and always strong) D and G bands that are characteristic for amorphous sp^2 -bonded carbon; those bands have been extensively studied and characterized in previous Raman studies of Stardust and are not the focus of this article. Rather, the present report is on the Raman information that can be obtained in addition to the confirmation that disordered carbonaceous material is present in Stardust. Some of the low wavenumber bands detected in this study (in addition to the D and G bands) could be assigned to the presence of the minerals olivine and pyrrhotite in one of the particles. The detection of these additional bands is unusual, because whenever there is amorphous sp^2 -bonded carbon present in a sample (no matter how much), it is very difficult to detect with Raman spectroscopy any other bonds (from either minerals or organic molecules) that are also present in the sample.

Most other detected bands, however, are unambiguously caused by the aerogel that was used in the collector cells of the Stardust mission. The particles of this study were pressed into an Au substrate, which probably made it especially difficult to find micrometer areas of the fragments that were aerogel-free. The peaks attributed to the aerogel are different for the two particles (coming from two different collector cells), but are identical and consistent among spectra taken of different fragments and/or areas of one given particle. Because of the aerogel contamination, interpretation of any organic bands that are not related to the sp^2 -hybridized carbon bond is impossible. But if any Stardust-related organics are present (in addition to the amorphous sp^2 -hybridized carbon), then there are two possibilities: (1) either they must be identical in nature to the ones present in the aerogel, because no additional organic bands were found in the particles above and beyond the ones that also were detected in the aerogel of the individual cells; or (2) they cannot be detected with Raman spectroscopy in the presence of amorphous sp^2 -bonded carbon. The latter is more likely, because vibrations from other organic bonds (C-H stretching, C-H twisting, C=O, etc.) usually cannot be detected in the presence of the sp^2 -hybridized carbon bond, even if the other organic bonds were

present in large concentrations. The reason for this is that the spectrum of sp^2 -bonded carbon is extremely strong and overwhelms any other organic Raman bands. Nevertheless, the organic aliphatic bands detected in this study were very strong; this is probably indirect confirmation that they come from outside the particles, and thus are due to aerogel contamination (rather than part of a native cometary material). Aliphatic C-H stretching bands previously were reported only for three other Stardust particles, but those aliphatic bands were not unambiguously related to aerogel contamination (Rotundi et al. 2008). This consistent and systematic finding of differences in the aerogel-related Raman peaks for all the spectra obtained of the two particles from this study leaves several possibilities: (1) the aerogel of the two cells (C2054 and C2092) was inherently different; (2) the cells themselves were heterogeneous on a millimeter scale in their aerogel properties and the impacting particles studied here hit different “types” of aerogel; and (3) the impacts themselves changed the properties/chemistry of the aerogel in a different way.

In conclusion, Raman analyses of Stardust particles mounted as “bulk” particles have to be interpreted with caution, because (1) aliphatic peaks in the C-H stretch region are likely to be caused by aerogel contamination, and (2) given that aerogel also has peaks in the spectral region of the bands for sp^2 -bonded carbon, it is possible that the shapes and/or intensities of D and G peaks are influenced by the aerogel peaks. In addition, surface coating of particles with sp^2 -bonded carbon makes it difficult (and usually impossible!) to detect any cometary inorganic mineral phases. Therefore, for all these reasons, it would be better to perform additional Raman studies not on individual whole particles (mounted on Au as it was the case in this study), but rather on particles that are “cracked open,” i.e., prepared as microtomed slices, so that the interior of a particle is made accessible to the laser beam and can be studied.

Acknowledgments—I thank the NASA curatorial staff at JSC, especially Keiko Nakamura-Messenger, for the very careful and excellent sample preparation and the excellent photodocumentation of the prepared particles. I also thank Darby Dyar who provided synthetic olivine standards, and Graciela Matrajt who provided ultramicrotomed thin-sections of Stardust particles Febo and Ada. Critical comments by Larry Nittler and an anonymous referee on a previous version of this manuscript are appreciated.

Editorial Handling—Dr. Scott Sandford

REFERENCES

- Al-Oweini R. and El-Rassy H. 2009. Synthesis and characterization by FTIR spectroscopy of silica aerogels prepared using several Si(OR)₄ and R''Si(OR')₃ presursors. *Journal of Molecular Structure* 919:140–145.
- Bonal L., Quirico E., Bourot-Denise M., and Montagnac G. 2006. Determination of the petrologic type of CV3 chondrites by Raman spectroscopy of included organic matter. *Geochimica et Cosmochimica Acta* 70:1849–1863.
- Bridges J. C., Burchell M. J., Changela H. C., Foster N. J., Creighton J. A., Carpenter J. D., Gurman S. J., Franchi I. A., and Busemann H. 2010. Iron oxides in comet 81P/Wild 2. *Meteoritics & Planetary Science* 45:55–72.
- Brownlee D., Tsou P., Anderson J. D., Hanner M. S., Newburn R. L., Sekanina Z., Clark B. C., Hörz F., Zolensky M. E., Kissel J., McDonnell J. A. M., Sandford S. A., and Tuzzolino A. J. 2003. Stardust: Comet and interstellar dust sample return mission. *Journal of Geophysical Research* 108:1–15.
- Brownlee D., Tsou P., Aléon J., Alexander C. M. O' D., Araki T., Bajt S., Baratta G. A., Bastien R., Bland P., Bleuet P., Borg J., Bradley J. P., Brearley A., Brenker F., Brennan S., Bridges J. C., Browning N., Brucato J. R., Brucato H., Bullock E., Burchell M. J., Busemann H., Butterworth A., Chaussidon M., Chevront A., Chi M., Cintala M. J., Clark B. C., Clemett S. J., Cody G., Colangeli L., Cooper G., Cordier P., Daghlian C., Dai Z., D'Hendecourt L., Djouadi Z., Dominguez G., Duxbury T., Dworkin J. P., Ebel D., Economou T. E., Faurey S. A. J., Fallon S., Ferrini G., Ferroir T., Fleckenstein H., Floss C., Flynn G., Franchi I. A., Fries M., Gainsforth Z., Gallien J.-P., Genge M., Gilles M. K., Gillet P., Gilmour J., Glavin D. P., Gounelle M., Grady M. M., Graham G. A., Grant P. G., Green S. F., Grossemy F., Grossman L., Grossman J., Guan Y., Hagiya K., Harvey R., Heck P., Herzog G. F., Hoppe P., Hörz F., Huth J., Hutcheon I. D., Ishii H., Ito M., Jacob D., Jacobsen C., Jacobsen S., Joswiak D., Kearsley A. T., Keller L., Khodja H., Kilcoyne A. L. D., Kissel J., Krot A., Langenhorst F., Lanzirotti A., Le L., Leshin L., Leitner J., Lemelle L., Leroux H., Liu M.-C., Luening K., Lyon I., MacPherson G., Marcus M. A., Marhas K., Matrajt G., Meibom A., Mennella V., Messenger K., Mikouchi T., Mostefaoui S., Nakamura T., Nakano T., Newville M., Nittler L. R., Ohnishi I., Ohsumi K., Okudaira K., Papanastassiou D. A., Palma R., Palumbo M. E., Pepin R. O., Perkins D., Perronnet M., Pianetta P., Rao W., Rietmeijer F., Robert F., Rost D., Rotundi A., Ryan R., Sandford S. A., Schwandt C. S., See T. H., Schlutter D., Sheffield-Parker J., Simionovici A., Simon S., Sittitsky I., Snead C. J., Spencer M. K., Stadermann F. J., Steele A., Stephan T., Stroud R., Susini J., Sutton S. R., Taheri M., Taylor S., Teslich N., Tomeoka K., Tomioka N., Toppani A., Trigo-Rodríguez J. M., Troadec D., Tsuchiyama A., Tuzolino A. J., Tyliczszak T., Uesugi K., Velbel M., Vellenga J., Vicenzi E., Vincze L., Warren J., Weber I., Weisberg M., Westphal A. J., Wirick S., Wooden D., Wopenka B., Wozniakiewicz P., Wright I., Yabuta H., Yano H., Young E. D., Zare R. N., Zega T., Ziegler K., Zimmerman L., Zinner E., and Zolensky M. 2006. Comet 81P/Wild 2 under a microscope. *Science* 314:1711–1716.
- Brunetto R., Borg J., Dartois E., Rietmeijer F. J. M., Grossemy F., Sandt C., d'Hendecourt L. S., Rotundi A., Dumas P., Djouadi Z., and Jamme F. 2011. Mid-IR, far-IR, Raman micro-spectroscopy, and FESEM-EDX study of IDP L2021C5: Clues to its origin. *Icarus* 212:896–910.
- Burchell M. J., Faurey S. A. J., Wozniakiewicz P., Brownlee D. E., Hörz F., Kearsley A. T., See T. H., Tsou P., Westphal A., Green S. F., Trigo-Rodríguez J. M., and Dominguez G. 2008. Characteristics of cometary dust tracks in Stardust aerogel and laboratory calibrations. *Meteoritics & Planetary Science* 43:23–40.
- Busemann H., Alexander C. M. O' D., and Nittler L. R. 2007. Characterization of insoluble organic matter in primitive meteorites by micro-Raman spectroscopy. *Meteoritics & Planetary Science* 42:1387–1416.
- Busemann H., Nguyen A. N., Cody G. D., Hoppe P., Kilcoyne A. L. D., Stroud R. M., Zega T. J., and Nittler L. R. 2009. Ultra-primitive interplanetary dust particles from comet 26P/Grigg-Skjellerup dust stream collection. *Earth and Planetary Science Letters* 288:44–57.
- De Gregorio B. T., Stroud R. M., Cody G. D., Nittler L. R., Kilcoyne A. L., and Wirick S. 2011. Correlated microanalysis of cometary organic grains returned by Stardust. *Meteoritics & Planetary Science* 46:1376–1396.
- Dyar M. D., Sklutke E. C., Menzies O. N., Bland P. A., Lindsley D., Glotch T., Lane M. D., Schaefer M. W., Wopenka B., Klima R., Bishop J. L., Hiroi T., Pieters C., and Sunshine J. 2009. Spectroscopic characteristics of synthetic olivines: An integrated multi-wavelength and multi-technique approach. *American Mineralogist* 94:883–898.
- Gallien J.-P., Khodja H., Herzog G. F., Taylor S., Koepsell E., Daghlian C. P., Flynn G. J., Sittitsky I., Lanzirotti A., Sutton S. R., and Keller L. P. 2008. Characterization of carbon- and nitrogen-rich particle fragments captured from comet 81P/Wild 2. *Meteoritics & Planetary Science* 43:335–351.
- Hörz F., Bastien R., Borg J., Bradley J. P., Bridges J. C., Brownlee D. E., Burchell M. J., Chi M., Cintala M. J., Dai Z. R., Djouadi Z., Dominguez G., Economou T. E., Faurey S. A. J., Floss C., Franchi I. A., Graham G. A., Green S. F., Heck P., Hoppe P., Huth J., Ishii H., Kearsley A. T., Kissel J., Leitner J., Leroux H., Marhas K., Messenger K., Schwandt C. S., See T. H., Snead C., Stadermann F. J., Stephan T., Stroud R., Teslich N., Trigo-Rodríguez J. M., Tuzzolino A. J., Troadec D., Tsou P., Warren J., Westphal A., Wozniakiewicz P., Wright I., and Zinner E. 2006. Impact features on Stardust: Implications for comet 81P/Wild 2 dust. *Science* 314:1716–1719.
- Kuebler K. E., Jolliff B. L., Wang A., and Haskin L. A. 2006. Extracting olivine (Fo-Fa) compositions from Raman spectral peak positions. *Geochimica et Cosmochimica Acta* 70:6201–6222.
- Matrajt G. and Brownlee D. 2006. Acrylic embedding of Stardust particles encased in aerogel. *Meteoritics & Planetary Science* 41:1715–1720.
- Matrajt G., Ito M., Wirick S., Messenger S., Brownlee D. E., Joswiak D., Flynn G., Sandford S., Snead C., and Westphal A. 2008. Carbon investigation of two Stardust particles: A TEM, NanoSIMS and XANES study. *Meteoritics & Planetary Science* 43:315–334.
- Mernagh T. P. and Trudu A. G. 1993. A laser Raman microprobe study of some geologically important sulphide minerals. *Chemical Geology* 103:113–127.
- Muñoz-Caro G. M., Matrajt G., Dartois E., Nuevo M., d'Hendecourt L., Deboffe D., Montagnac G., Chauvin N., Boukari C., and Le Du D. 2006. Nature and evolution of the dominant carbonaceous matter in interplanetary dust

- particles: Effects of irradiation and identification with a type of amorphous carbon. *Astronomy & Astrophysics* 459:147–159.
- Muñoz-Caro G. M., Dartois E., and Nakamura-Messenger K. 2008. Characterization of the carbon component in cometary Stardust samples by means of infrared and Raman spectroscopy. *Astronomy & Astrophysics* 485:743–751.
- Pasteris J. 1998. The laser Raman microprobe as a tool for the economic geologist. In *Applications of microanalytical techniques to understanding mineralizing processes*, edited by McKibben M. A., Shanks W. C., and Ridley W. I. Littleton, Colorado: Society of Economic Geologists. pp. 233–250.
- Pasteris J. D., Wopenka B., Freeman J. J., Young V. L., and Brandon H. J. 1999. Analysis of breast implant capsular tissue for crystalline silica and other refractile phases. *Plastic and Reconstructive Surgery* 103:1273–1276.
- Quirico E., Borg J., Raynal P.-I., Montagnac G., and d'Hendecourt L. 2005. A micro-Raman survey of 10 IDPs and 6 carbonaceous chondrites. *Planetary and Space Science* 53:1443–1448.
- Riegel B., Hartmann I., Kiefer W., Groß J., and Fricke J. 1997. Raman spectroscopy on silica aerogels. *Journal of Non-Crystalline Solids* 211:294–298.
- Rotundi A., Baratta G. A., Borg J., Brucato J. R., Busemann H., Colangeli L., d'Hendecourt L., Djouadi Z., Ferrini G., Franchi I. A., Fries M., Grossemy F., Keller L. P., Mennella V., Nakamura K., Nittler L. R., Palumbo M. E., Sandford S. A., Steele A., and Wopenka B. 2008. Combined micro-Raman, micro-infrared, and field emission scanning electron microscope analyses of Comet 81P/Wild 2 particles collected by Stardust. *Meteoritics & Planetary Science* 43:367–397.
- Sandford S. A., Aléon J., Alexander C. M. O'D., Araki T., Bajt S., Baratta G. A., Borg J., Bradley J. P., Brownlee D. E., Brucato J. R., Burchell M. J., Busemann H., Butterworth A., Clemett S. J., Cody G., Colangeli L., Cooper G., d'Hendecourt L., Djouadi Z., Dworkin J. P., Ferrini G., Fleckenstein H., Flynn G. J., Franchi I. A., Fries M., Gilles M. K., Glavin D. P., Gounelle M., Grossemy F., Jacobsen C., Keller L. P., Kilcoyne A. L. D., Leitner J., Matrajt G., Meiborn A., Mennella V., Mostefaoui S., Nittler L. R., Palumbo M. E., Papanastassiou D. A., Robert F., Rotundi A., Snead C. J., Spencer M. K., Stadermann F. J., Steele A., Stephan T., Tsou P., Tylliszczak T., Westphal A. J., Wirrick S., Wopenka B., Yabuta H., Zare R. N., and Zolensky M. E. 2006. Organics captured from comet 81P/Wild 2 by the Stardust spacecraft. *Science* 314:1720–1724.
- Sandford S. A., Bajt S., Clemett S. J., Cody G., Cooper G., De Gregorio B. T., de Vera V., Dworkin J. P., Elsila J. E., Flynn G. J., Glavin D. P., Lanzirrotti A., Limerio T., Martin M. P., Snead C. J., Spencer M. K., Stephan T., Westphal A. J., Wirrick S., Zare R. N., and Zolensky M. E. 2010. Assessment and control of organic and other contaminants associated with the Stardust sample return from comet 81P/Wild 2. *Meteoritics & Planetary Science* 45:406–433.
- Steele A., Fries M., Amundsen H. E. F., Mysen B., Fogel M., Schweizer M., and Boctor N. 2006. A comprehensive imaging and Raman spectroscopy study of ALH 84001 and a terrestrial analogue from Svalbard (abstract #2096). 37th Lunar and Planetary Science Conference. CD-ROM.
- Trigo-Rodríguez J. M., Domínguez G., Burchell M. J., Hörz F., and Llorca J. 2008. Bulbous tracks arising from hypervelocity capture in aerogel. *Meteoritics & Planetary Science* 43:75–86.
- Tsou P. 1995. Silica aerogel captures cosmic dust intact. *Journal of Non-Crystalline Solids* 186:415–427.
- Tsou P., Brownlee D. E., Anderson J. D., Bhaskaran S., Chevront A. R., Clark B. C., Duxbury T., Economou T., Green S. F., Hanner M. S., Hörz F., Kissel J., McDonnell J. A. M., Newburn R. L., Ryan R. E., Sandford S. A., Sekanina Z., Tuzzolino A. J., Vellinga J. M., and Zolensky M. E. 2004. Stardust encounters comet 81P/Wild 2. *Journal of Geophysical Research* 109:1–8.
- Walrafen G. E., Hokmabadi M. S., Holmes N. C., Nellis W. J., and Henning S. 1985. Raman spectrum and structure of silica aerogel. *The Journal of Chemical Physics* 82:2472–2476.
- Wang A., Kuebler K., Jolliff B., and Haskin L. 2004. Mineralogy of a Martian meteorite as determined by Raman spectroscopy. *Journal of Raman Spectroscopy* 35:504–514.
- Westphal A. J., Snead C., Butterworth A., Graham G. A., Bradley J. P., Bajt S., Grant P. G., Bench G., Brennan S., and Pianetta P. 2004. Aerogel keystones: Extraction of complete hypervelocity impact events from aerogel collectors. *Meteoritics & Planetary Science* 39:1375–1386.
- Wopenka B. 1988. Raman observations on individual interplanetary dust particles. *Earth and Planetary Science Letters* 88:221–231.
- Wopenka B., Matrajt G., Joswiak D., and Brownlee D. 2007. A new sample preparation method that is ideal for the Raman analysis of stardust, IDPs and other samples that contain disordered carbonaceous material (abstract). *Meteoritics & Planetary Science* 42:A166.
- Wopenka B., Matrajt G., Bajt S., Joswiak D., and Brownlee D. 2008. Carbonaceous phases are different in individual stardust particles: FTIR and Raman spectra of Febo and Ada (abstract #1827). 39th Lunar and Planetary Science Conference. CD-ROM.
- Zolensky M., Nakamura-Messenger K., Fletcher L., and See T. 2008. Curation, spacecraft recovery, and preliminary examination for the Stardust mission: A perspective from the curatorial facility. *Meteoritics & Planetary Science* 43:5–21.